International Materials Reviews

ISSN: 0950-6608 (Print) 1743-2804 (Online) Journal homepage: http://www.tandfonline.com/loi/yimr20

Microfluidic synthesis of functional inorganic micro-/nanoparticles and applications in biomedical engineering

Nanjing Hao, Yuan Nie & John X. J. Zhang

To cite this article: Nanjing Hao, Yuan Nie & John X. J. Zhang (2018) Microfluidic synthesis of functional inorganic micro-/nanoparticles and applications in biomedical engineering, International Materials Reviews, 63:8, 461-487, DOI: 10.1080/09506608.2018.1434452

To link to this article: https://doi.org/10.1080/09506608.2018.1434452

Published online: 08 Feb 2018.

INTERNATIONAL MATERIALS REVIEWS
2018, VOL. 63, NO. 8, 461–487
https://doi.org/10.1080/09506608.2018.1434452

The Institute of Materials, Minerals and Mining
ASM INTERNATIONAL
Taylor & Francis
Taylor & Francis Group

FULL CRITICAL REVIEW

Check for updates

Microfluidic synthesis of functional inorganic micro-/nanoparticles and applications in biomedical engineering

Nanjing Hao, Yuan Nie and John X. J. Zhang

Thayer School of Engineering, Dartmouth College, Hanover, NH, USA

ABSTRACT

Engineered micro-/nanoparticles of various physicochemical properties play significant roles in biomedical engineering from biosensing, in vivo imaging, in vitro diagnosis, drug delivery to therapy. Compared to conventional batch synthesis, microfluidics-based synthesis enables precise reaction control, enhanced mixing, and rapid chemical reactions, allowing for the flow synthesis of particles in a controllable, sustainable, and costsaving manner that is attractive to industry. This review focuses on the recent advances of using microfluidic devices for the flow synthesis of inorganic micro-/nanoparticles with specific properties and their practical applications. We highlight the principle and the merits of emerging microfluidic techniques over conventional methods, discuss chemical reactions performed in the microfluidic reactors, summarize and tabulate strategies for the flow synthesis of inorganic particles, and provide the established applications of materials from these microfluidic systems. The challenges, opportunities, and future perspectives of microfluidics in the synthesis and applications of inorganic micro-/nanoparticles are furthermore discussed.

ARTICLE HISTORY
Received 26 June 2017
Accepted 23 January 2018

KEYWORDS
Microfluidic; microreactor; inorganic; micro-/nanoparticle; physicochemical properties; flow synthesis; mixing; biomedical engineering

Introduction

Micro-/nanoparticles are being considered as of critical importance in versatile emerging frontiers, such as nanoelectronics, biosensors, cancer theranostics, molecular catalysis, and alternative energy. In each of these fields, the physicochemical properties of particles such as size, shape, composition, and surface chemistry can be systematically exploited to optimise their efficacy in terms of dispersity, stability, reactivity, compatibility, electronic, magnetic, optical, or fluorescent behaviour. All these cases require to have efficient, controllable, and reproducible techniques for the synthesis of micro-/nanoparticles with well-defined properties [1,2]. Over the years a variety of synthetic methodologies have been developed for producing micro-/nanoparticles. These methods can be generally grouped into two main categories: the top-down approach and the bottom-up approach. The former approach is to mechanically break down large-sized products into micrometer-/nanometer-sized particles by sonication, milling, high-pressure homogenisation, extrusion, etc., while the latter approach involves the condensation of atoms, monomers, or molecular components to assemble micro-/nanoparticles by polymerisation, sol–gel reaction, microemulsion, co-precipitation, hydrolysis, etc. Within the paradigm of the top-down approach and the bottom-up approach, numerous kinds of micro-/nanoparticles have been produced. However, these conventional batch synthesis methods always tend to suffer from a lack of precise control of the mixing, nucleation, and growth processes, and thus irreproducibility of final physicochemical properties of micro-/nanoparticles from batch to batch.

Microfluidics-based flow synthesis offers a variety of advantages over the conventional batch synthesis [3–6]. First of all, hydrodynamic focusing inside microreactors enables the continuous synthesis of micro-/nanoparticles with well-defined properties due to the sufficient and intensive mixing of reagent solutions, which also allows for fast screening and optimisation of the synthesis parameters. Second, the batch-to-batch difference among different tests and microreactors is relatively small, showing great capabilities for performing complex parallel processing and scale-up. Third, the large surface-to-volume ratio of microfluidic channels provides enhanced mass and heat transfer, which enable chemical reactions to be performed with higher yields in small volume than conventional batch methods. Fourth, microfluidic devices provide fine operation of each step during automating multistep synthesis, and there is great potential to combine chemical reactions, purification, and analysis together in a single microchip for realising the 'lab-on-chip' design. Moreover, microreactors could work at elevated pressures and temperatures while confining potentially toxic, flammable, and explosive staring materials, which gives great chances to create novel micro-/nanostructured materials. With the smart

CONTACT John X. J. Zhang john.zhang@dartmouth.edu Thayer School of Engineering, Dartmouth College, 14 Engineering Drive, Hanover, NH 03755, USA

design and construction of microreactors, recent studies employed microfluidics for controllable synthesis and application of micro-/nanomaterials with desired and predetermined structures. These functional materials that can be produced in a well-controlled, reproducible, and high-throughput manner demonstrated superior performance in many fields, such as low sensing detection limit, high catalysis activity, targeted cancer imaging, and enhanced therapeutic efficiency. In addition, microfluidic technologies acting as a robust platform for rapid screening of micro-/nanoparticles offer a great way to accelerate the clinical translation of these functional materials.

This review focuses primarily on the research and development of microfluidics-based flow synthesis and biomedical applications of inorganic micro-/nanoparticles, emphasising progress during the last two decades. Reviews of the microfluidic synthesis of organic materials, such as liposome, hydrogel, and polymer-based ones, are already available [7–11]. The review is organised as follows. In the first section, an overview of current established microfluidic reactors is provided. Then, the flow synthesis of various kinds of inorganic micro-/nanoparticles, such as metal, metal oxide, metal salts, quantum dots (QDs), silica, and hybrid composite, using the unique capabilities of microfluidic devices is described. Next, the specific applications of these manufactured particles in sensing, catalysis, imaging, drug delivery, and theranostics fields are introduced to highlight the promising features of microfluidic synthesis. Finally, the last section presents the in-depth discussion on current challenges and future perspectives of microfluidics-based flow synthesis techniques for inorganic micro-/nanostructures.

Microfluidics-based reaction systems: categories and principals

Microfluidics is defined as the miniaturised systems that manipulate nanoliter to microliter fluids in channels with dimensions of tens to hundreds of micrometers [12]. Owing to the scale-down effects, microfluidics technology offers many great benefits such as low consumption of samples and reagents, low cost, high-throughput, rapid mass and heat transport, and precise control of fluids at micro-/nanoscale [13]. The advent of microfluidics technology provides great opportunities in the fields of analytic and synthetic chemistry. Microfluidic reactors (or microreactors in short) which are miniaturised devices designed specifically for chemistry synthesis, can facilitate the synthesis process via precise control of reaction parameters and optimisation of the production of the chemicals [14].

Generally, microreactors for chemistry synthesis could be grouped into three main categories: continuous laminar flow reactors, segmented flow reactors, and droplet-based reactors. Continuous laminar flow microreactors are relatively simple to design and easy to manipulate and to scale-up. But it has the inherent problems with the parabolic velocity profile and residence time distributions [15]. These problems could be solved with segmented flow microreactors to a certain extent. However, segmented flow microreactors suffer from physical contact of the reagents and the wall, which may lead to contamination of the products. With droplet-based microreactors, the cross-contamination problems could be avoided. But droplet-based microreactors require careful consideration towards geometry design for the generation of droplets, which may hinder the scale-up of the synthesis process [15]. Other methods such as photolithography-based synthesis and supraparticles synthesis using assembly of colloids can also be used for chemical synthesis of inorganic particles, but they will not be discussed in this review [7].

Specifically, continuous laminar flow microreactors involve only single phase liquid flows (Figure 1(A)). Multiple liquid reagents (such as LR1 and LR2) of different compositions and concentrations are pumped into the microfluidic systems through the inlets. In these laminar-dominant microreactors, mixing is a key process to control for the optimisation of productions. Peclet number (*Pe*), which is a dimensionless number defined as the ratio of convection over diffusion, could be used to estimate the channel dimensions required for mixing under different reaction conditions. Some common mixing modules for 2D micromixers design are winding microchannels and distributive mixing-based micromixers as shown in Figure 1(A) [16].

Segmented flow microreactors usually include several liquid phase flows for the reagents and one gas phase flow to create gas 'bubbles' for the isolation of different segments of reagents (Figure 1(B)). The gas 'bubbles' are generated because of differences in surface tension between gas and liquid phases, and they are useful in confining reactions in liquid segments. In a typical design (Figure 1(B)), two or more reagents in liquid phases (LR1, LR2 …) are introduced into the microreactor through the inlets. Extra mixing sections could be added into the design for different reaction requirements. Segmented flow microreactors may have contamination problems due to physical contact of the reagents and the channel walls. These problems could be avoided to some extent by thorough considerations towards the hydrophobicity of the channel walls.

Compared with laminar flow microreactors and segmented flow microreactors, one of the biggest advantages with droplet-based microreactors is compartmentalisation, with which rapid mixing, a good control of time and reagents, and contamination-free microenvironment could be achieved. Droplet-based microreactors are one type of multiphase flow

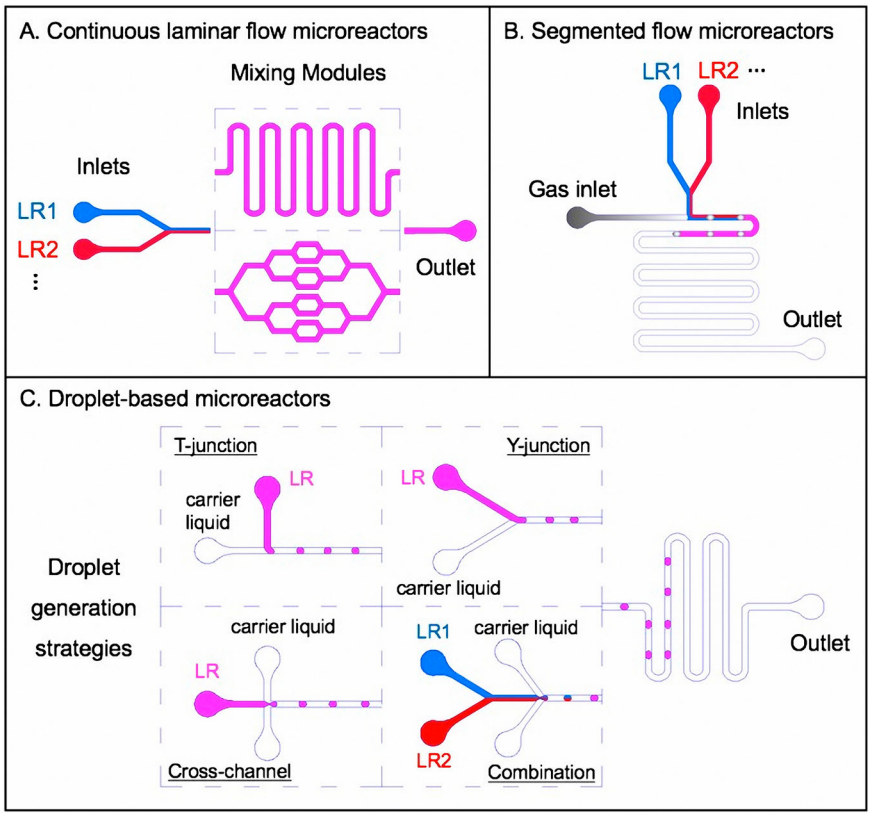

Figure 1. Three main categories of microreactors: (A) continuous laminar flow microreactors, in which single phase flows of different liquid reagents (LR1, LR2 …) are introduced into the systems through the inlets, going through subsequent mixing modules such as winding microchannels and distributive mixing based mixers; (B) segmented flow microreactors, which usually consist of several liquid phase flows for introducing certain reagents (LR1, LR2 …) and one gas phase flow to create 'bubbles' for separating segments of reagents; and (C) droplet-based microreactors, with which different strategies for droplets generation could be developed, including T-junction, Y-junction, cross-channel, and a combination of several simple designs such as the Y-junction and the cross-channel for more complicated reactions.

microreactors that generally include several liquid phase flows of reagents and an immiscible liquid phase flow as carrier liquid for the generation of droplets (Figure 1(C)). For droplet creation, a dimensionless capillary number $Ca = \eta V/\gamma$ which describes the competition between surface tension and viscous effect needs to be considered. Above a critical value of Ca, droplets break-off occurs. As shown in Figure 1(C), some typical geometry designs for droplet generation include T-junction, Y-junction, cross-channel flow-focusing, and a combination of several simple strategies such as Y-junction and cross-channel for more complicated reactions. T-junction and Y-junction are relatively simple designs, in which droplet size depends on channel width and flow rate. Therefore, reaction process could be manipulated easily in these droplet-based microreactors. In cross-channel flow-focusing microreactors, geometry and flow conditions must be optimised to yield regular sized droplets for chemical synthesis [7]. Electrohydrodynamic method, which includes dielectrophoresis-driven and electrowetting on dielectric methods, is another droplet generation strategy. Droplet-based microreactors are versatile microsystems for chemistry synthesis. Manipulation of droplets such as fission, fusion, mixing, and sorting can largely facilitate the fabrication of micro/nanoparticles under different reaction conditions. However, for droplets generation, the hydrophobicity of channel walls still needs to be considered. Non-stick condition of either the continuous phase or the dispersed phase to channel walls should be satisfied for better performance of the droplet-based microreactors [17].

The development of microreactors followed the gradually growing demand for the synthesis of nanoparticles. The simplest designs started with tubular microreactors made of stainless steel, glass, and polymers [18–20] that fell into all the three groups of microreactors. They had the advantages of low cost and easy scaling up. However, they could not meet the needs for more complicated reactions, which stimulated the progress of chip-based microreactors [21]. The combination of tubular and chip-based microreactors has also been employed in some cases to meet the synthesis requirements [22]. However, there is still a lot of room in microfluidic synthesis of nanomaterials in general, of inorganic functional nanoparticles in particular, which is of interests to this review. The next generation of microreactors will be application-directed and will further develop towards more integrated, automated, modular, and multistage

microsystems. The great potentials of microfluidics in biomedical applications will also propel the translation of microreactors from academia towards industry. Though demonstrated with some examples [23,24], microfluidic synthesis for industrial purpose is still at its infancy. The choices will be made between scaling up or scaling out, considering the performance of the output.

As discussed above, three main types of microreactors work under different principles with advantages and disadvantages. Choices among these microreactors depend on various applications such as high-throughput screening, measuring kinetics, optimising reaction conditions, and multiple-step reactions [25,26]. Overall, the existence of microfluidics-based reaction systems has greatly promoted the development of chemistry synthesis in many aspects such as from macro to micro, expensive to low cost, time-consuming to fast, and irreproducible to easy scale-up.

Microfluidic synthesis of inorganic materials at micro-/nanoscale

Inorganic micro-/nanoparticles show different physical, chemical, optical, and thermal properties compared with their bulk solids. To date, various wet chemical methods have been developed for the synthesis of inorganic micro-/nanomaterials, such as sol–gel processing, co-precipitation, hydrothermal, templated synthesis, and solvothermal processing. This section reviews current approaches for the microfluidic synthesis of different micro-/nanoparticles, including metals, metal oxides, metal salts, QDs, silica, and hybrid composites.

Metals, metal oxides, and metal salts

Gold and silver

Gold and silver nanoparticles constitute two of the most extensively studied types of nanomaterials because of their straightforward synthesis, high stability, and attractive optoelectronic properties. Both gold and silver particles could generate localised surface plasmon response upon light irradiation, a unique effect that is sensitive to the local dielectric environment. This phenomenon endows them great opportunities to be widely utilised in sensing, catalysis, and cancer theranostics fields. In all cases, the availability of gold and silver nanoparticles with well-controlled physicochemical properties is an essential prerequisite for application consideration.

Microfluidic reactors can provide precisely tuneable parameters to produce size-, shape-, and surface-controllable gold and silver nanoparticles for potential biomedical applications (Figure 2(A)). Flow synthesis of gold and silver nanoparticles has already been successfully performed in laminar- (Figure 2(B)), segmented- (Figure 2(C)), and droplet-based microreactors (Figure 2(D)) at room temperature to mild temperature conditions (Table 1) [18,27,28]. A number of surfactants and ligands systems have been employed to stabilise the as-synthesised particles and minimise agglomeration inside microfluidic channels [29,30]. These systems include thiols [31], PVP [30], PEG [19], and ionic liquids [32]. Similar as batch methods, microfluidic synthesis of gold and silver nanoparticles can be generally realised by reduction of metal salt solutions (such as $HAuCl_4$ and $AgNO_3$) with sodium borohydride or ascorbic acid, but the products from microreactors generally exhibit enhanced sensing sensitivity, catalysis activity, and/or theranostic efficiency. The working features of microreactors, such as flow rate, reaction time, and temperature, were found important to tailor the structures of the resultant products [18,27]. Currently, besides well-established spherical gold and silver particles with narrow size distributions, rod-shaped particles with various aspect ratios [19,28,33,34], hexagon-shaped particles [35], hollow particles [36], fibre and belt particles [37] have also been successfully fabricated via different microfluidic platforms. In addition, given microfluidic system allows the implementation of multi-stages for particles production, scale-up synthesis of functionalised gold and silver particles and inline optical monitoring of the synthesis process for parameters optimisation become available (Figure 2(E)) [33,36]. To address the surface adhesion of gold/silver particles or their nuclei on microfluidic channels, methods such as silanisation and pH-adjustment were explored to minimise the fouling [29,38]. Alternatively, gold and silver structures can be also intentionally formed and patterned on the inner surface of microfluidic channels for real-time surface-enhanced Raman scattering (SERS) sensing applications (Figure 2(F)) [39,40]. In addition, more and more evidences revealed that the reaction rate of microfluidic synthesis is nearly tens of times than that of batch synthesis, and the resultant products in microreactor exhibited at least two times narrower size distributions than those obtained in a batch reactor [38].

Magnetic particles (iron oxide, cobalt, and nickel)

Magnetic particles constitute an important type of micro-/nanomaterials that display unique magnetic properties when subjected to external magnetic fields. This special capacity allows them to gain increasing research interests in areas including sensing, biomedical imaging, site-specific drug delivery, diagnosis, and biological samples labelling and sorting. For all these applications, physicochemical properties, such as particle size, shape, dispersity, surface chemistry, and magnetism, are again important factors determining the scopes and effectiveness of implementation.

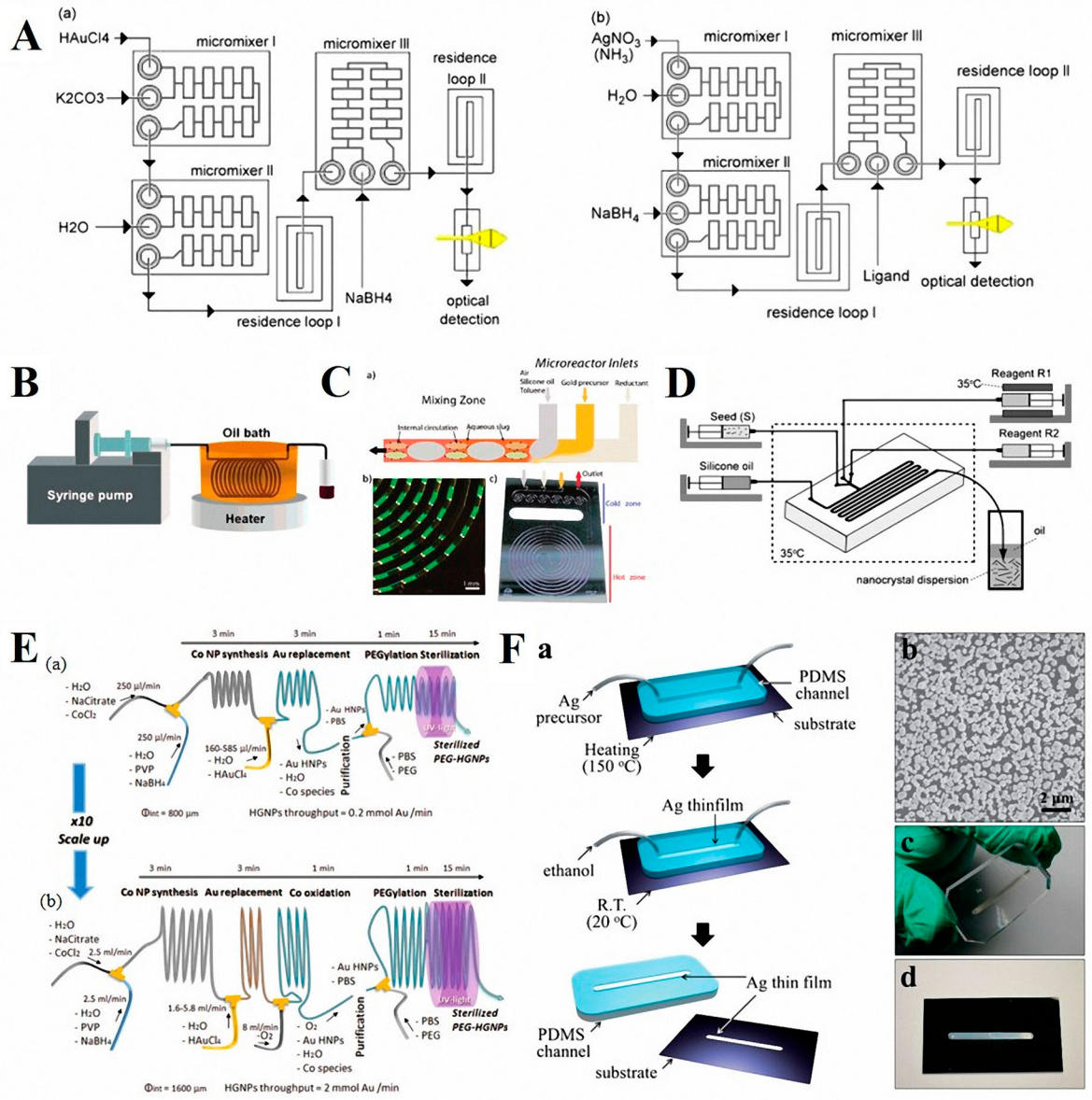

Figure 2. Microfluidic systems for gold and silver particles synthesis. (A) Modular microreactor arrangement for flow-through process: (a) synthesis of gold nanoparticles and (b) synthesis of silver nanoparticles [29]. (B) Experimental setup of the synthesis of Ag nanoparticles in a tubular microreactor [18]. (C) Spiral silicon/Pyrex microfluidic reactor designed for the segmented flow generation of gold nanocrystal [27]. (D) Schematic of the droplet-based microfluidic experimental setup [28]. (E) (a) Scheme of the experimental set-up to produce hollow gold nanoparticles. (b) Microfluidic scaled up set-up for a 10 times higher hollow gold nanoparticles throughput [36]. (F) (a) A schematic diagram of the microfluidic patterning system. The Ag precursor is injected into the channel and an Ag thin film is formed. (b) A SEM image of an Ag thin film fabricated in a channel. (c) A photograph of an Ag-patterned PDMS channel. (d) A photograph of an Ag-patterned Si wafer [40]. All images reproduced with permission.

Microfluidic techniques provide great beneficial for minimising local variations of synthetic parameters and have already been applied to the synthesis of different kinds of magnetic particles, including iron oxide, nickel, and cobalt (Table 1). Among them, iron oxide (Fe_3O_4 or Fe_2O_3) particles have attracted relatively more research attention. Of the available microfluidic synthesis methods, co-precipitation (Figure 3(A)) and thermal decomposition (Figure 3(B)) are two of the most common methods used to produce iron oxide particles for biomedical applications [72,74]. The impacts of the flow parameters, such as linear velocity of fluid, residence time, and reactor dimension, on the particle size distribution were systematically investigated [74]. Flow synthesis of nickel particles can be realised by aqueous reduction of nickel salt solutions (such as $NiCl_2$ and $NiSO_4$) with hydrazine as a reducing agent and sodium hydroxide as a catalyst (Figure 3(C)) [73,75]. The size distribution, morphology, and crystal structure of nickel particles can be well-controlled by tuning the flow rates of microreactors [75]. Cobalt particles are another kind of magnetic materials that are known to exist in three polymorphs, *i.e.* face-centered cubic (fcc), hexagonally close-packed (hcp), and epsilon (ε) phases. These three different crystal structures can be facilely synthesised in a microfluidic

Table 1. Examples of metals, metal oxides, and metal salts micro-/nanoparticles synthesised in microfluidic devices.

Particle type	Microreactor type	Particle property	Reaction condition	Key precursors	Ref
Gold/Silver (by year)					
Ag	Tubular reactor	5.6–8.7 nm	100–140°C; 0.08–0.7 mL min^{-1}	$C_2F_5CO_2Ag$ + TOA	2004[18]
Au	Split-and-recombine mixer	5–50 nm	R.T.; 0.5–8 mL min^{-1}	$HAuCl_4$+AA	2005[38]
Ag	PTFE capillary reactor	6.7–16.8 nm	170°C; 56–130 µL min^{-1}	Ag(OAc)+oleylamine	2005[41]
Au; Ag	Tubular reactor	~20 × 50 nm; rod	30–50°C; 4–150 µL min^{-1}	$HAuCl_4$+$AgNO_3$+CTAB + AA	2006[33]
Au	Radial interdigitated mixer	~3–4 nm	R.T.; 400–800 µL min^{-1}	$HAuCl_4$+DDT	2007[31]
Au; Ag	Split-and-recombine mixer	4–7 nm	R.T.; 200–8000 µL min^{-1}	$HAuCl_4$+$AgNO_3$+$NaBH_4$	2007[29]
Au	Multichannel micromixer	~1 nm	273 K; 25–200 mL h^{-1}	$HAuCl_4$+$NaBH_4$+PVP	2008[30]
Au	Pneumatic rotary micromixer	35 nm; hexagon	115°C; ~5–8 µL min^{-1}	$HAuCl_4$+TSC	2008[35]
Ag	PTFE capillary reactor	4.8–8.1 nm	170°C; 14.2–282.8 µL min^{-1}	Ag(OAc)+oleylamine	2008[42]
Au; Ag	Y-shaped reactor	~2 nm	R.T.	$HAuCl_4$+$AgNO_3$+$NaBH_4$+TSC	2009[43]
Au	T-junction reactor	10–50 nm; sphere, rod, sharp-edged	35°C; 2.5–20 µL min^{-1}	$HAuCl_4$+$AgNO_3$+CTAB + AA	2009[28]
Au	Serpentine micromixer	4.38 nm	R.T.; 500–900 µL h^{-1}	$HAuCl_4$+$NaBH_4$+MID	2010[32]
Au	Y-shaped mixer	20–40 nm	R.T.; 50–200 Hz	$HAuCl_4$+TSC	2010[44]
Au	Vortex-type micromixer	19–58 nm	100°C; 10 psi; 170 µL min^{-1}	$HAuCl_4$+TSC	2010[45]
Au	LTCC-based reactor	2.7–3.8 nm	25°C; 10–100 µL min^{-1}	$HAuCl_4$+$NaBH_4$+MUA	2010[46]
Au	Droplet-based bioreactor	~10 nm	R.T.; 1.5 µL min^{-1}	$HAuCl_3$	2012[47]
Au; Ag	T-junction reactor	3.73–4.28 nm	R.T.; 0.5 mL h^{-1}	$HAuCl_4$+$AgBF_4$+$NaBH_4$+MID	2012[48]
Au	Segmented flow reactor	2.8–4.9 nm	100°C; 27–300 µL min^{-1}	$HAuCl_4$+$NaBH_4$	2012[27]
Au	T-junction reactor	1–2 nm	100°C; 80 µL min^{-1}	$HAuCl_4$+TSC	2012[49]
Ag	T-junction reactor	3–15 nm	90°C; 200–600 µL min^{-1}	$AgNO_3$+*C. Platycladi* extract	2012[50]
Ag	Segmented flow reactor	5–20 nm	90°C; 35–1000 µL min^{-1}	$AgNO_3$+KOH + oleic acid	2012[51]
Au	Y-shaped mixer	2–50 nm; sphere, rod	R.T.; 50 mL min^{-1}	$HAuCl_4$+$NaBH_4$	2013[34]
Au	Straight channel	125–140 nm	22–50°C; ~5 µL (*In situ*)	$HAuCl_4$+PDMS	2013[39]
Au	SWCNT-based reactor	~100 nm	R.T.; 0.05 µL min^{-1}; –0.8 V	$HAuCl_4$	2013[52]
Ag	Microwave-integrated reactor	4.3 nm	1 mL min^{-1}; microwave (30W)	$[Ag(NH_3)_2]^+$+Glucose + PVP	2013[53]
Ag	Electrode-patterned reactor	100–150 nm × 1 µm; vertical wall-shaped	1–4 µL min^{-1}; –2.7 V	$AgNO_3$+$Cu(OAc)_2$+CTAB	2013[54]
Ag	Segmented flow reactor	~50 nm (triangular)	R.T.	$AgNO_3$+$NaBH_4$+AA	2013[55]
Au	PTFE capillary reactor	24–36 nm	40–80°C; 0.041–3.63 mL min^{-1}	$HAuCl_4$	2014[56]
Ag	Straight channel	Thin film	150°C; 10 µL min^{-1} (*In situ*)	$AgNO_3$+PVP + EG	2014[40]
Au	Y-shaped mixer	32.4 nm; hollow	R.T.; 25 mL h^{-1}	$CoCl_2$+ $HAuCl_4$+$NaBH_4$+PVP	2014[36]
Au	Three-jet microreactor	59 nm; meatball-like	R.T.; 5–70 µL min^{-1}	$HAuCl_4$+AA + NaBr	2015[57]
Ag	Straight channel	~50–100 nm	R.T.–180°C; 5 µL min^{-1} (*In situ*)	$AgNO_3$+EG	2015[58]
Ag	Three-inlet microchannel	30 nm–5 µm; fibre, sphere, belt, cluster	R.T.; 15–60 µL min^{-1}	$AgNO_3$+o-phenylenediamine	2015[37]
Au	Segmented flow reactor	2.5–4 nm	R.T.; 12.5–400 µL min^{-1}	$HAuCl_4$	2015[59]
Au	Y-shaped multistage reactor	10–50 nm; sphere, rod	R.T.; 0.62–5.85 mL h^{-1}	$HAuCl_4$+$NaBH_4$+CTAB + AA	2016[19]
Ag	Droplet-based reactor	3–22 nm	R.T.; 10–30 mL h^{-1}	$AgNO_3$+$NaBH_4$	2016[60]
Ag	Crack-based nanochannel	Belt	25–45°C	$AgNO_3$+KOH + Glucose	2017[61]
Au	Y-shaped mixer	~11.5 nm	0.05 mL min^{-1}	$HAuCl_4$+TSC + TA	2017[62]
Au	Glass capillary reactor	48–135 nm	R.T.; 15–60 mL h^{-1}	$HAuCl_4$+AA + PVP	2017[63]
Au	Y-shaped mixer	~1 nm	R.T.; N_2; 2.6 L h^{-1}	$HAuCl_4$+$NaBH_4$+PVP	2017[64]
Magnetic particles (by year)					
Fe_2O_3	Glass capillary reactor	10–60 nm	210°C; 2–30 mL h^{-1}	$Fe(NO_3)_3$+Formamide	2005[65]
Co	Y-shaped mixer	3.5–4.7 nm; 39–124 emu g^{-1}	R.T.; N_2; 0.08–0.9 mL min^{-1}	$CoCl_2$+$LiBEt_3H$ + SB12	2006[66]
Fe_3O_4	Electrode-patterned reactor	~4 nm	200 V, 30 kHz; 30–800 µL h^{-1}	$FeCl_3$+ $FeCl_2$+NH_4OH	2008[67]
Fe_2O_3	PTFE capillary reactor	~6 nm	R.T.; 10–400 µL min^{-1}	$FeCl_3$+ $FeCl_2$+TMAOH	2008[68]
Co	Y-shaped mixer	2.84–4.69 nm	20–50°C; 0.08–0.9 mL min^{-1}	$CoCl_2$+$LiBEt_3H$ + SB12	2008[69]
Fe_3O_4	Double-loop micromixer	4.83–6.69 nm; 7 emu g^{-1}	R.T.; 5–20 psi; <680 µL min^{-1}	$FeCl_3$+ $FeCl_2$+NaOH	2009[70]
Co	IRCMP-based reactor	3.5–4.7 nm	4–50°C; 0.08–0.9 mL min^{-1}	$CoCl_2$+$LiBEt_3H$ + SB12	2009[71]

(*Continued*)

Table 1. Continued.

Particle type	Microreactor type	Particle property	Reaction condition	Key precursors	Ref
Fe_3O_4	Droplet-based bioreactor	4.42 nm	R.T.; 1.5 μL min^{-1}	$FeCl_2$	2012[47]
Fe_3O_4	PTFE capillary reactor	3.6 nm; 58 emu g^{-1}	60°C; 67–600 μL min^{-1}	$FeCl_3$+ $FeCl_2$+NH_4OH	2012[72]
Ni	T-shaped mixer	5.4–9.2 nm; 5.1 emu g^{-1}	60–120°C; 3 mL min^{-1}	$NiCl_2$+N_2H_4+NaOH	2012[73]
Co	Y-shaped mixer	~30 nm	R.T.; 15 mL h^{-1}	$CoCl_2$+$NaBH_4$+PVP	2014[36]
Fe_3O_4	T-shaped mixer	4.6 nm	250°C; 33bar; 0.19–6.6 mL min^{-1}	$Fe(acac)_3$+oleylamine + PEG	2015[74]
Ni	T-shaped mixer	15–83 nm	80°C; 0.1–40 mL min^{-1}	$NiSO_4$+N_2H_4+NaOH + PVP	2015[75]
Fe_2O_3/Fe_3O_4	T-shaped mixer	~10 nm	2.5–5 mL min^{-1}	$FeCl_3$+ $FeCl_2$+NaOH	2017[76]
Fe_3O_4	Stainless steel microreactor	<4 nm	180–280°C; 0.25–1 mL min^{-1}	$Fe(acac)_3$+TEG	2018[77]
Other metals, metal oxides, and metal salts (by particle type)					
AuPd	Interdigital multilaminar reactor; cyclone micromixer	0.9–2.8 nm	R.T.; 1.92–2.6 L h^{-1}	$HAuCl_4$+H_2PdCl_4/K_2PdCl_4	2014[78] 2018[79]
Au@Ag	Combinatorial capillary; CDrAG-based reactor	~16 nm	R.T.; 0.063–58.9 μL min^{-1}	$HAuCl_4$+$AgNO_3$	2013[80,81]
$BaSO_4$	T-shaped mixer; MTMCR	10–150 nm	R.T.; 20 μL min^{-1}–9 L min^{-1}	$BaCl_2$+$(NH_4)_2SO_4$/Na_2SO_4/H_2SO_4	2007[82], 2008[83,84], 2009[85]
$CaCO_3$	Liquid–gas dual phase reactor	30 nm (solid); 350 nm (hollow)	R.T.; CO_2; 0.2 μL min^{-1}–240 mL min^{-1}	$Ca(OH)_2$+CO_2	2012[86], 2013[87]
CoSm	Y-shaped mixer	~5 nm	2–50°C; N_2	$CoCl_2$+$SmCl_3$	2009[88]
Cu	T-shaped mixer; Y-shaped mixer	2–135.6 nm	R.T.; 0.06 mL–110 L h^{-1}	$CuSO_4$/$CuCl_2$/ [Cu$(NH_3)_4$]·$(OH)_2$	2005[89], 2010[90], 2011[91,92], 2014[93]
Cu_2O	Y-shaped mixer	~200–2000nm; sphere, star-like, flower-like	40°C; 50–300 μL min^{-1}	$CuSO_4$+N_2H_4+NaOH	2010[94]
Cu@Cu_2O	Multichannel tubular reactor	6–14 nm	R.T.; 0.1–40 mL min^{-1}	$CuSO_4$+$NaBH_4$+PVP	2015[95]
Cu–CuO	Counter-current flow reactor	~10 nm	20 mL min^{-1}	$CuSO_4$+$NaBH_4$	2017[96]
FeCo	Y-shaped mixer	<5 nm	0–90°C; 0.2–3 mL min^{-1}	$CoCl_2$+$FeCl_2$+$NaBH_4$	2014[97]
FeMn	Y-shaped mixer	~5 nm	R.T.; 4–15 μL min^{-1}	$FeSO_4$+$MnCl_2$	2012[98]
FeOOH	Microtubular reactor; droplet-based reactor	7–40 nm × 30–400 nm; rod	60°C; 0.5–400 μL min^{-1}	$FeCl_3$+TMAOH	2009[99,100], 2011[101]
Pd	Y-shaped mixer; serpentine reactor; glass capillary reactor	1–6.4 nm; worm-like, sphere	R.T.–200°C; 2.5–1000 μL min^{-1}	$PdCl_2$+$LiBEt_3H$/$Pd(OAc)_2$	2010[102,103], 2015[104]
Pt	Y-shaped mixer	2.4–8.2 nm; worm-like, sphere	R.T.; 80 μL min^{-1}	$PtCl_2$+$LiBEt_3H$	2010[102]
PtBi	Capillary reactor	4–33.5 nm; sphere, rod	200–350°C; N_2	$Bi(NO_3)_3$+H_2PtCl_6	2015[105]
Ru	Y-shaped mixer	2.5–4.8 nm; worm-like, sphere	R.T.; 80 μL min^{-1}	$RuCl_3$+$LiBEt_3H$	2010[102]
TiO_2	Y-shaped mixer; Glass capillary reactor	~2–100 nm; sphere, rod	R.T.; ~0.6–200 μL min^{-1}	TTIP	2002[106], 2004[107], 2007[108], 2009[109], 2011[110]
WO_3	Droplet-based reactor	<3 nm	25–120°C; 20–120 mL h^{-1}	WCl_6+BnOH	2013[111]
ZnO	Segmented flow reactor; Y-shaped mixer	20 nm–4 μm; flower-like, sphere, spindle, sheet	60–150°C; 500–5000 μL min^{-1}	$Zn(Ac)_2$/$Zn(NO_3)_2$+NaOH	2013[112], 2017[113]

Abbreviations: AA: ascorbic acid; CDrAG: concentration-gradient droplet array generator; CTAB: cetyltrimethylammonium bromide; DDT: 1-dodecanethiol; EG: ethylene glycol; IRCMP: *in situ* rapidly cooling microfluidic process; LTCC: low-temperature co-fired ceramics technology; MID: 1-methylimidazole; MTMCR: microporous tube-in-tube microchannel reactor; MUA: 11-mercaptoundecanoic acid; PDMS: polydimethylsiloxane; PTFE: polytetrafluoroethylene; PVP: poly (vinylpyrrolidinone); SB12: 3-(N,N-dimethyldodecylammonia)propanesulfonate; SWCNT: single-walled carbon nanotubes; TA: tannic acid; TEG: triethylene glycol; TMAOH: tetramethylammonium hydroxide; TOA: trioctylamine; TSC: trisodium citrate; TTIP: titanium tetraisoproxide.

reactor through manipulation of the flow rates (Figure 3(D)) [66]. Typical microfluidic synthesis of cobalt particles involves reducing cobalt salts (such as $CoCl_2$) with reducing agents, such as sodium borohydride ($NaBH_4$) [36], or a mixture of lithium hydrotriethylborate ($LiBet_3H$) and 3-(N,N-dimethyldodecylammonia)propanesulfonate (SB12) [66,69,71].

Others

In addition to the above-mentioned extensively studied gold, silver, and magnetic particles, many other kinds of metals, metal oxides, and metal salts have been successfully synthesised through microreactors (Table 1). Among them, platinum [102], palladium [102–104], copper [89–93], and titanium dioxide [106–110] have gained increasing attentions due to their specific catalytic capacities. When compared with these kinds of particles synthesised by conventional batch approaches, the microfluidic approaches endow particles with a smaller size and narrower size distribution, which dramatically enhanced the catalytic activities. Some kinds of metal salts particles, such as $CaCO_3$ [86,87] and $BaSO_4$[82–85], were also prepared with controllable size by simply varying the flow rate. It is noting that bimetallic alloy (such as AuPd [78], CoSm [88], FeCo [97], and FeMn [98]) and core–

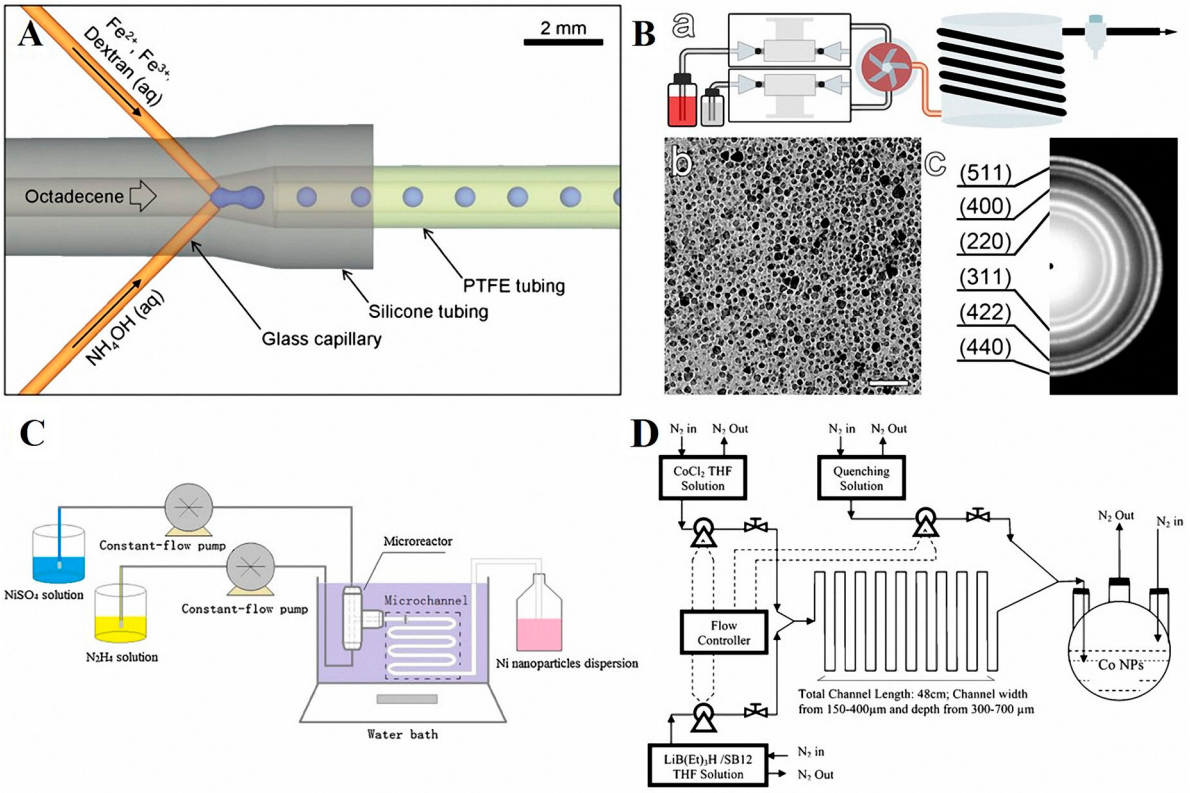

Figure 3. Microfluidic systems for magnetic particles synthesis. (A) Schematic of the capillary-based droplet reactor showing the injection of separate precursor streams of Fe^{2+}/Fe^{3+}/dextran and NH_4OH into a continuous stream of octadecene carrier fluid; iron oxide nanoparticles are formed inside the droplets [72]. (B) Flow synthesis of Fe_3O_4 nanoparticles prepared by a residence time of 12 min, at 250°C and under 33 bar using a 2.1 mm wide and 3.8 m long tube reactor (the scale bar corresponds to 50 nm) [74]. (C) Schematic of the synthesis processes of nickel nanoparticles by continuous-flow microreactor [75]. (D) Schematic of the microfluidic reactor process for phase-controlled synthesis of cobalt nanoparticles [66]. All images reproduced with permission.

shell metallic particles (such as $Cu@Cu_2O$ [95]) having a high quality can be facilely produced in a flow system, their synergistic combination gives improved performance for many applications (as also discussed in the section 'Hybrid composites').

Quantum dots

QDs are luminescent semiconductor nanoparticles having many potential and established applications in areas such as optics, electronics, sensors, imaging, and diagnostics. QDs can, for example, show broad optical excitation and narrow emission, and are less susceptible to photobleaching. These unique properties rely in particular on particle size as well as particle shape and surface chemistry. Therefore, much effort has been made to produce QDs with well-defined physicochemical properties. Given their precise temperature and pressure control and enhanced mass and heat transfer, microfluidics-based devices have already been widely employed to synthesise QDs [114].

CdS and CdSe are two kinds of the most intensively studied nanocrystals using microfluidic reactors (Table 2). The flow synthesis of CdS can be realised at room temperature by the redox reactions of cadmium salts (such as $Cd(NO_3)_2$ and $CdCl_2$) with Na_2S [115–118]. CdSe nanocrystals are often synthesised using a surfactant (such as trioctyl phosphine and trioctyl phosphine oxide) at high temperature (~200–300°C) [119–122]. Different types of microfluidic devices, such as glass capillary [123,124], silica capillary [125], PTFE capillary [126,127], and droplet-based reactor [128], have been developed to produce high-quality QDs. To increase the relatively low fluorescence quantum yields, a surface capping layer (such as ZnS from Zinc diethyldithiocarbamate precursor) is generally used to deposit on QDs surface for forming core–shell structures [125,128]. Conventional batch methods, single-phase laminar flow capillary reactors, and segmented flow reactors for CdSe QDs synthesis at atmospheric pressure always suffer from limited numbers of high-boiling-point solvents, slow mixing, broad residence time distributions, and thus leading to broad size distributions. Therefore, high-pressure microreactor has also been created for narrow size QDs synthesis in supercritical fluids, overcoming some of the limitations of high-boiling-point solvents (expensive, low diffusivity, high viscosity, and limited choice of precursors due to solubility consideration) (Figure 4(A)) [129]. In addition, different surface

Table 2. Examples of QDs particles synthesised in microfluidic devices.

Particle type	Microreactor type	Particle property	Reaction condition	Key precursors	Ref
CdS	Split-and-recombine mixer	3.2–12 nm	R.T.; 10–300 μL min^{-1}	$Cd(NO_3)_2$+Na_2S	2002[115]
CdSe	Glass capillary reactor	2–4.5 nm	245–275°C; 0.25 mL min^{-1}	$Cd(OAc)_2$+Se + TOPO + TOP	2002[119]
CdSe	Convective mixer	1.52–2.70 nm	180–320°C; 2–30 μL min^{-1}	$Cd(OH)_2$+Se + TOP + oleic acid	2003[135]
CdSe	Serpentine micromixer	2.23–2.69 nm	180–210°C; 1.5–3 μL min^{-1}	$Cd(CH_3)_2$+Se + TOPO + TBP	2003[136]
CdSe@ZnS	Y-type micromixer		220–300°C; 100 μL min^{-1}	$Cd(OAc)_2$+Se + TOPO + TOP + ZnS	2004[137]
CdSe	Glass capillary reactor	~1–1.5 nm	220–270°C; 0.25–10 μL min^{-1}	$Cd(OAc)_2$+Se + TOPO + TOP	2004[123]
CdSe	Glass capillary reactor	~2 nm	90–150°C	$Cd(OAc)_2$+Se + TOPO + TOP	2004[124]
CdSe	Glass capillary reactor	~1–5 nm	210–330°C; 0.05–1 mL min^{-1}	$Cd(OAc)_2$+Se + TOPO + TOP	2004[120]
CdS; CdS@CdSe	Serpentine micromixer		R.T.; 4–16 μL min^{-1}	$CdCl_2$+Na_2S + Na_2Se	2004[116]
CdSe@ZnS	Silica capillary reactor	~2–5 nm	150–240°C	$Cd(OAc)_2$+Se + ZDC	2005[125]
CdSe	Segmented flow reactor		260–280°C; 10–100 μL min^{-1}	$Cd(OH)_2$+Se + TOP + oleic acid	2005[138]
CdSe	Cross-shaped reactor	3.4 nm	240–300°C; 0.1–10 μL min^{-1}	CdO + Se + TOP + oleic acid	2005[21]
CdS	Double T- junction device	4.2–8.2 nm	R.T.; <6 μL min^{-1}	$Cd(NO_3)_2$+NaS	2006[117]
CdSe	Y-shaped reactor		160–255°C; ~2–40 μL min^{-1}	CdO + Se + TOP + oleic acid	2007[139]
CdS	Y-shaped reactor	2–4 nm; Cys-capped	R.T.; 0.7–4 μL min^{-1}	$CdSO_4$+Na_2S + Cys	2007[131]
CdSe	PTFE capillary reactor	2.5–4.3 nm	255–295°C; 100 μL min^{-1}	CdO + Se + TOP + oleic acid	2007[121]
CdSe	High-pressure microreactor	~3–6 nm	210–270°C; 5 MPa	$Cd(acac)_2$+Se + TOP + oleic acid	2008[129]
CdSe	PTFE capillary reactor	2.5–4.5 nm	230–285°C; 149 μL min^{-1}	CdO + Se + TOP + oleic acid	2008[126]
CdSe; CdSe@ZnS	PTFE capillary reactor	2.4–3.6 nm	120–285°C	CdO + Se + ZDC	2008[128]
CdS	PTFE capillary reactor	3.0–5.4 nm	220°C; 2.22–17.8 mL h^{-1}	CdO + S+oleic acid	2009[127]
CdSe	PTFE capillary reactor	3.6 nm	280°C	CdO + Se + TOP + oleic acid	2009[140]
ZnS@CdSe@ZnS	Glass capillary reactor	5.5 nm	150–240°C; 10 μL min^{-1}	$Cd(OAc)_2$+Se + ZDC	2009[141]
CdSe	PTFE capillary reactor	2.1–4.0 nm	240–300°C; 8.92 mL h^{-1}	CdO + Se + TOPO + TOP	2009[142]
InP	Glass capillary reactor	~5 nm	170–230°C; 4–60 μL min^{-1}	InCl3 + TTMSP + ZU	2009[143]
CdSe	Combinatorial glass capillary	~2–4.5 nm	195–300°C; 94.2 μL min^{-1}	$Cd(OAc)_2$+Se + TOP + oleic acid	2010[133]
CdTe@ZnS	Y-shaped reactor	~1.5–3 nm; Man-/Gal-capped	90–160°C; 33.33 μL min^{-1}	CdO + Se + TOP + DEZ	2010[130]
ZnSe@ZnS	Serpentine micromixer	3–4 nm	220°C; 5–30 μL min^{-1}	$Zn(OAc)_2$+Se + TOP + oleyamine	2012[144]
CdSe	Droplet-based bioreactor	5 nm	R.T.; 1.5 μL min^{-1}	$CdCl_2$+SeO_2	2012[47]
CdTe; CdSe; CdSeTe	Multichannel droplet reactor	~2.5 nm	175–195°C; 2–5 mL min^{-1}	CdO + Se + Te + TOP + oleic acid	2013[122]
PbS; PbSe	Droplet-based capillary mixer	3.8–4.5 nm	95–145°C; 20 μL min^{-1}	$(Pb(OAc)_2$+TMS_2S + Se	2014[145]
CdTe	Serpentine micromixer	1.5 nm; BSA-capped	50–100°C; 500 μL min^{-1}	$Cd(ClO_4)_2$+Te + MPA + BSA	2014[132]
CdS	Droplet-based reactor	3.2 nm	R.T.; 5.4 μL h^{-1}	$CdCl_2$+Na_2S + MPA	2015[118]
PbS	Droplet-based reactor	2–6 nm	80–150°C; 30–60 μL min^{-1}	$(Pb(OAc)_2$+TMS_2S	2015[134]
CdSe	Y-shaped reactor	~3–5 nm	240–270°C; 424.1 μL min^{-1}	CdO + Se + TOP + oleic acid	2016[146]
CdSe	Y-shaped reactor	~4 nm	210–280°C; 50 μL min^{-1}	CdO + Se + TOP + oleic acid	2016[147]
CdS	Y-shaped reactor	2.4–3.7 nm	375–5000 μL min^{-1}	$CdCl_2$+S + oleyamine	2017[148]
CdSe	PTFE capillary reactor	2.57–4.31 nm; vague angular, tripodia, polygon, sphere	150–300°C; 0.6 mL min^{-1}	CdO + Se + TOP + oleic acid	2017[149]
CdSe	Split-and-recombine mixer	3–10 nm	250°C; 50–600 μL min^{-1}	$Cd(OAc)_2$+Se + TOP + oleic acid	2017[150]
CdSe	Droplet-based reactor	1.6–2.6 nm	<250°C	CdO + Se + TOP + oleic acid	2018[151]

Abbreviations: BSA: bovine serum albumin; Cys: cysteine; DEZ: diethylzinc; Gal: galactose; Man: mannose; MPA: 3-mercaptopropionic acid; PTFE: polytetrafluoroethylene; TBP: tributylphosphine; TMS_2S: bis(trimethylsilyl)sulfide; TOP: trioctyl phosphine; TOPO: trioctyl phosphine oxide; TTMSP: tris(trimethylsilyl)phosphine; ZDC: zinc diethyldithiocarbamate; ZU: zinc undecylenate.

ligands, including carbohydrates (Figure 4(B)) [130], amino acids [131], and proteins [132], can be successfully conjugated onto QDs via continuous-flow microreactors, the obtained biofunctionalised QDs are known to be useful targeted fluorescent labels for bioimaging [132]. Microreactors offer significant

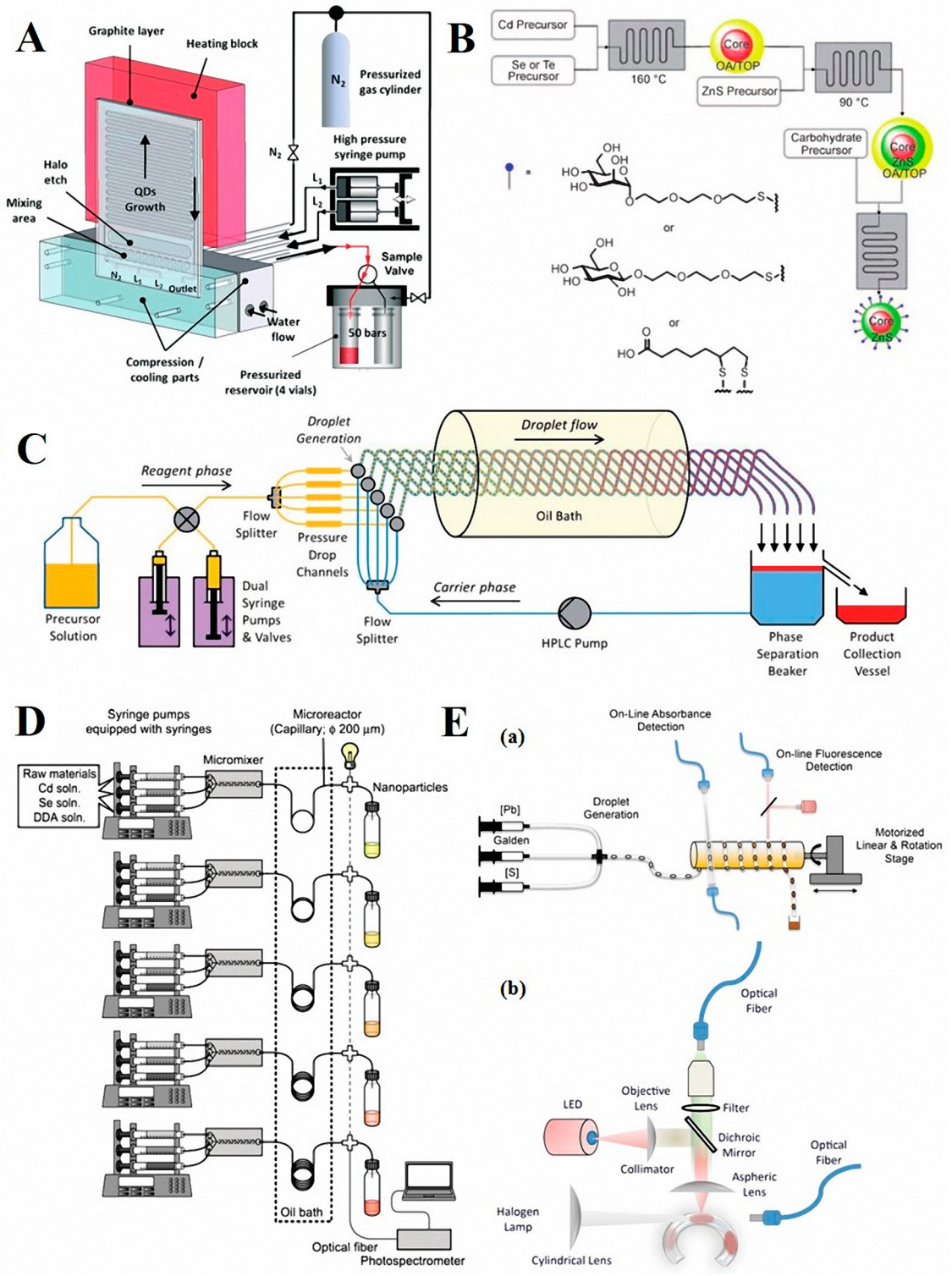

Figure 4. Microfluidic systems for QDs synthesis. (A) High-pressure and high-temperature microreactor comprising a compression-cooling aluminium part, a high-pressure syringe pump, a 5-way high-pressure valve, and a high-pressure reservoir containing four vials, for supercritical continuous-flow synthesis of CdSe QDs [129]. (B) Microreactor setup for the continuous-flow synthesis of carbohydrate-functionalised QDs [130]. (C) Large-scale synthesis of nanocrystals in a multichannel droplet reactor [122]. (D) Schematic representation of the combinatorial synthesis system for CdSe nanoparticles [133]. (E) Schematic of the droplet-based microfluidic platform integrated with inline absorbance and fluorescence detection for kinetic analysis of PbS quantum dot synthesis [134]. All images reproduced with permission.

advantages over equivalent batch reactions, most notably in terms of and enhanced mass transfer rates to the order of 10–1000 times as compared to batch reactors and increased reaction control [96], which can be utilised for large-scale synthesis of QDs in a multichannel droplet reactor (Figure 4(C)) [122]. A production rate of over 100 g per day can be easily achieved at a milliliter-per-minute flow rate scale. Microreactors integrated with an inline detector analysis system have also been developed to enable the concurrent

investigation of the emission characteristics of QDs and a real-time estimation of their size and concentration during nucleation and growth (Figure 4(D,E)) [133,134]. These combinatorial platforms allow for fast and reliable extraction of the reaction kinetics during materials synthesis and the resulting physicochemical properties of new micro-/nanoparticles.

Silica (SiO_2)

Silica micro-/nanoparticle as one of the another most extensively investigated inorganic materials has been attracting great interests because of its wide potential applications in various fields. Silica materials have relatively high thermal and mechanical stability, tuneable structure, good dispersability, and facile surface functionalisation. Among different silica formats, mesoporous silica materials are especially attractive due to their high surface-to-volume ratio, rich porous texture, and adjustable pore types and pore size distribution [152–157]. In addition, silica matrix can be also widely and easily employed for coating or encapsulating metals, metal oxides, and QDs to form different kinds of hybrid composites and thus showing multifunctional properties (As discussed in the next section).

Since 2004, different sized and shaped silica micro-/nanoparticles were successfully synthesised using microfluidic techniques (Table 3), and a series of geometric parameters and experimental conditions were investigated. The influence of microreactor design on silica particle size distributions was first examined between laminar flow reactor and segmented flow reactor (Figure 5(A)). Laminar flow reactors are affected by axial dispersion at high linear velocities and thus leading to wide particle size distributions, whereas segmented flow reactor could eliminate the axial dispersion by creating the internal recirculation in the liquid plugs and thus produce a narrow size distribution of silica particles [158,159]. However, compared to batch based process, both laminar flow reactor and segmented flow reactor produce silica particles with narrower size distributions and higher

Table 3. Examples of silica micro-/nanoparticles synthesised in microfluidic devices.

Particle type	Microreactor type	Particle property	Reaction condition	Key precursors	Ref
Solid-SiO_2	Laminar flow reactor; segmented flow reactor	164–540 nm; sphere	R.T.; 4–30 μL min^{-1}	TEOS + NH_4OH	2004[158]
Solid-SiO_2	Laminar flow reactor; segmented flow reactor	~300 nm; sphere	R.T.; 10–30 μL min^{-1}	TEOS + NH_4OH	2004[159]
Meso-SiO_2	T-shaped device	~1 μm; sphere; 6.4 nm (pore)	R.T.–80°C; 70 mTorr; 0.5–3.5 μL min^{-1}	TEOS + HCl + P104	2008[163]
Meso-SiO_2	T-shaped device	~20 μm; sphere; ~5–15 nm (pore)	R.T.; ~0.3–16.5 μL min^{-1}	TEOS + HCl + P104	2008[164]
Solid-SiO_2	T-junction reactor	Sphere: 0.25–0.5 mm; Rod:1.1 mm × 2.3–4.7 mm	R.T.; 0.005–1 mL min^{-1}	TEOS + HCl + TTAB	2008[169]
Colloidosome	Glass capillary reactor	~30 μm; nonspherical with internal voids	R.T.; 1500–35000 μL h^{-1}	15 nm SNPs + PVA + Toluene	2009[172]
Meso-SiO_2	Cross-channel device	130 μm; hollow sphere; 2 nm (pore)	R.T.; 0.12–1.4 mL h^{-1}	TEOS + CTAB + NH_4OH	2010[168]
Meso-SiO_2	Coupled co-flow device	1–15 μm; sphere; 2.4 nm (pore)	R.T.; 0.19–0.32 μL s^{-1}	TMOS + HNO_3+NH_4OH + PDFO	2010[173]
Bubble	Glass capillary reactor	29 μm; hollow sphere	R.T.; 82.7 kPa; 1000–120000 μL h^{-1}	15 nm SNPs + PVA + Toluene	2010[174]
Meso-SiO_2	Coupled co-flow device	1–5 μm; sphere; 2.4 nm (pore)	65°C	TMOS + HNO_3+NH_4OH + PDFO	2010[175]
Solid-SiO_2	Baffled micromixer	46–250 nm; sphere	25–55°C; 0.1–35 mL h^{-1}	TEOS + NH_4OH	2011[162]
Solid-SiO_2	Serpentine micromixer	7–50 μm; doughnut shape	R.T.; 0.02–5 mL h^{-1}	TEOS + TEA	2011[170]
Solid-SiO_2	Laminar flow reactor; segmented flow reactor	63–176 nm; sphere	R.T.; 0.075–20 μL min^{-1}	TMOS + PEI + HCl	2011[160]
Solid-SiO_2	Interdigital micromixer	~170 nm; sphere	30–60°C; 9.4 mL h^{-1}	TEOS + NH_4OH	2011[161]
Solid-SiO_2	Droplet-based reactor	50–350 nm; fluorescent sphere	R.T.; 0.003–0.5 μL s^{-1}	TEOS + APTES + FITC + NH_4OH	2012[176]
Meso-SiO_2	Glass capillary reactor	1.4–14.6 μm; hollow sphere; 7.44 nm (pore)	R.T.; 4–16 psi	TEOS + F127 + PMMA + THF	2012[165]
Solid-SiO_2	T-junction reactor	~100 μm; raspberry-like	50–60°C	TEOS + $NaHCO_3$+HCl + ABIL EM 90	2013[171]
Meso-SiO_2	Droplet-based reactor	7.7 μm; sphere; 3.4–6 nm (pore)	R.T.; 0.1–1 μL min^{-1}	TEOS + CTAB + HCl + ABIL EM 90	2013[166]
Solid-SiO_2	Droplet-based reactor	90–185 μm; sphere, hollow sphere, filbert-like	R.T.–60°C; 0.5–5 mL h^{-1}	TEOS + HCl + FAME + KOH	2014[177]
Meso-SiO_2	Interdigital micromixer; T-shaped mixer	50–650 nm; sphere, hollow sphere; ~3–4 nm (pore)	0–85°C; 0.03–1.2 mL min^{-1}	TEOS/TMOS + CTAB + NH_4OH/NaOH	2015[167]
Meso-SiO_2	Droplet-based reactor	~10–30 μm; sphere	50–300 μL h^{-1}	TEOS + P123 + HNO_3	2017[178]
Meso-SiO_2	Spiral-shaped reactor	80–150 nm; hollow ellipsoid; ~3 nm (pore)	R.T.; 100 μL min^{-1}	EMSN + BSA + PBS	2017[179]
Meso-SiO_2	Spiral-shaped reactor	~800 nm; hollow sphere	R.T.; 400 μL min^{-1}	TEOS + NH_4OH + CTAB	2017[180]
Meso-SiO_2	Spiral-shaped reactor	~130 nm–3 μm; fibre; ~3 nm (pore)	R.T.; 10–100 μL min^{-1}	TEOS + NH_4OH + CTAB	2018[181]

Abbreviations: APTES: aminopropyl triethoxysilane; BSA: bovine serum albumin; CTAB: cetyltrimethylammonium bromide; EMSN: ellipsoidal mesoporous silica nanoparticle; FAME: fatty acid methyl ester; FITC: fluorescein isothiocyanate; Meso-SiO_2: mesoporous silica; PDFO: pentadecaflouoro-1-octanol; PEI: polyethylenimine; PMMA: poly(methyl methacrylate); PVA: poly(vinyl alcohol); R.T.: room temperature; SNPs: silica nanoparticles; TEA: triethyl amine; TEOS: tetraethylorthosilicate; THF: tetrahydrofuran; TMOS: tetramethoxysilicate; TTAB: tetratrimethylammonium bromide.

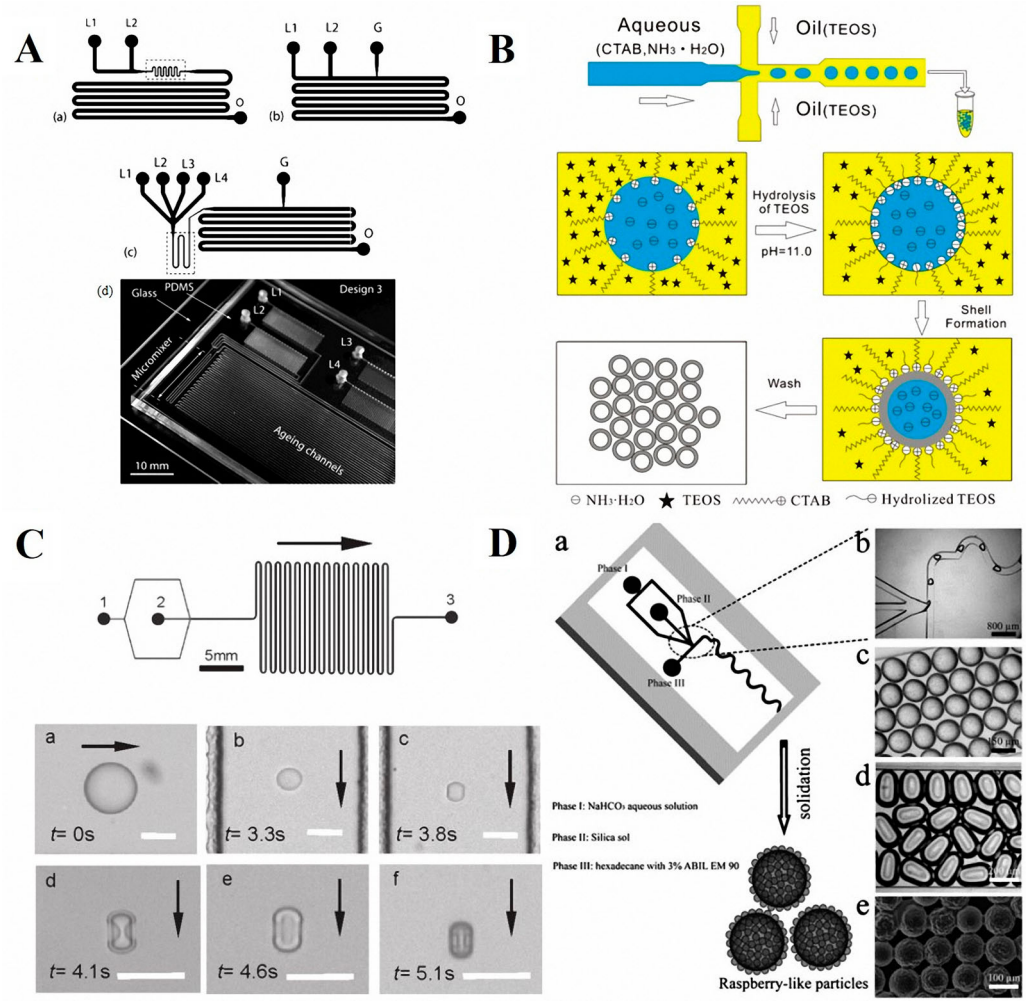

Figure 5. Microfluidic systems for silica particles synthesis. (A) Schematics of different microfluidic channels: (a) Design 1 (laminar flow reactor) has two liquid inlets (L1 and L2) and one outlet (O). (b) Design 2 (segmented flow reactor) has two liquid inlets (L1 and L2), a gas inlet (G), and an outlet (O). (c) Design 3 (segmented flow reactor) has four liquid inlets (L1–L4), a gas inlet (G), and an outlet (O). (d) Photograph of segmented flow microreactor (design 3): L1–L4 are the liquid inlets [158]. (B) Schematic illustration of the droplet microfluidic approach for preparing monodisperse hollow silica microspheres [168]. (C) Schematic of the PDMS device used for the synthesis of doughnut-shaped silica microparticles (top). Evolution of a droplet (bottom) as it travels downstream: (a) droplet generation; (b) shrinkage; (c) deformation; (d) buckling; (e) condensation; and (f) solidification [170]. (D) Microfluidic fabrication of raspberry-like silica particles. (a) Microfluidic device for forming silica particles. (b) Optical micrographs showing the formation of uniform precursor droplets at the T-junction; (c) optical micrographs of uniform spherical gel particles collected at the outlet of the microfluidic device; (d) optical micrographs of uniform ellipsoid gel particles; (e) SEM image of raspberry-like silica particles formed after solidification [171]. All images reproduced with permission.

particle yields [160], and the synthesis reproducibility and the TEOS conversion were also higher when using microreactors compared with batch reactors for the same synthesis times. These can be attributed to the shorter nucleation times and a greater homogeneity of microreactors [161]. The size of solid silica particles can be further adjusted by means of flow rate, reaction time, and temperature [162]. Similar as conventional batch synthesis, mesoporous silica particles can be also fabricated in microreactors at the presence of surfactants, such as triblock copolymer P104 [163,164], triblock copolymer F127 [165], and cationic surfactant cetyltrimethylammonium bromide (CTAB) [166,167]. In addition, combining sol–gel chemistry with microfluidic droplet-based techniques can lead to the hollow silica structures (Figure 5(B)), which are generally formed via hydrolysis and polymerisation of silica precursors (such as TEOS and TMOS) at the interface of water-in-oil droplets [165,168]. By adjusting the constrained geometry of the microfluidic devices, the shapes of silica particles can be also easily tuned from sphere to nonspherical morphology, such as rod [169], doughnut-like (Figure 5(C)) [170], and raspberry-like (Figure 5(D)) [171].

Hybrid composites

Microfluidic techniques allow for the uniformly and continuously incremental addition of reagents into multiple solution streams at different reaction stages, which provide great opportunities to facilitate the

synthesis of hybrid micro-/nanocomposites under more controllable and consistent conditions [182]. Combining the different inorganic–inorganic or inorganic–organic materials properties together are also of particular interest for diverse applications. This section aims to give a brief overview of hybrid structures recently developed using microfluidics. Table 4 summarises examples of hybrid micro-/nanocomposites synthesised in microfluidic devices.

Core–shell, Janus, and doping structures are three common types of hybrid composites that can be yielded from microfluidic techniques (Figure 6). For the flow synthesis of core–shell structures, the association of microreactors in series allows a simple way to add shell-forming reagents to a reacting phase containing core particles. Different kinds of inorganic–inorganic (Figure 6(A)) and inorganic–organic (Figure 6(B)) core–shell structures have already been successfully synthesised, such as Au@Ag [186], CdS@CdSe [116], CdSe@ZnS [125], CdTe@ZnS [130], Cu@Cu_2O [95], Fe_2O_3@SiO_2[99], SiO_2@Au [22], SiO_2@TiO_2[199], ZnSe@ZnS [144], Chitosan@Au [217], Chitosan@TS-1/Fe_3O_4/TiO_2[218], and SiO_2@Dextran [232]. Microreactors can be also easily applied for multistep processes with fast mixing and controllable residence time between each single mixing step, which can be used for the generation of multishell composites, such as Au@Ag@Au [187] and ZnS@CdSe@ZnS [141]. Therefore, microfluidic systems open great opportunities for constructing a series of multishell micro-/nanocomposites that are not easily realised from conventional batch methods. Janus particles exhibit interesting anisotropic properties due to their distinctly asymmetric structures and chemical compositions. Droplet-based microreactors are commonly employed to produce Janus particles of controllable size, shape, and composition (Figure 6(C,D)). Generally, the co-flow of two immiscible fluids containing monomers/polymers and inorganic components can be quickly cross-linked through different processes, such as UV [234], pH, and heating [235], after they have been placed in contact with each other. By confining the assembled drops in microchannels of varying geometry, bicompartmental Janus particles with different shapes can be produced continuously and uniformly (Figure 6 (C)) [234]. With the aid of gravity and externally applied forces, the components inside the droplets can be spatially positioned and multicompartmental Janus structures can be thus easily produced (Figure 6(D)) [235]. Doping structure that mixes the unique features of inorganic and inorganic/organic materials is another kind of well-established composite from microfluidic reactors (Table 4). In addition to the inorganic–inorganic doping (such as above-mentioned alloys [78,88,97,105]), inorganic–organic doping (such as metal-microcapsule (Figure 6(E)), and metal–organic framework (Figure 6(F)) via microreactors have recently attracted great attentions since it can yield uniform and stable composite for improving the overall performance, such as catalysis [224], drug delivery [230,232], and antibacteria [203], which will be also discussed in the following sections.

Applications of microfluidics-based inorganic micro-/nanoparticles

Various kinds of inorganic micro-/nanoparticles, including metals, metal oxides, metal salts, QDs, silica, and hybrid composites have been successfully synthesised through microreactors. The systematic reaction control and enhanced mixing process of microfluidic systems endow these materials with superior structural and surface properties compared to conventional batch synthesis approaches. Practically, microfluidics-based micro-/nanoparticles have already played significant roles in advancing the opportunities in several applied fields, such as biosensing and detection, molecular catalysis, and biomedicine.

Biosensing and assay-on-particles detection

Due to their low-cost fabrication and high-throughput, microfluidics-based sensing is of great interest for a wide range of scientists from physicists to chemists to biologists. Microfluidic platforms permit detection of small volume of desired samples as well as low target analyte concentrations that are generally not possible with conventional testing platforms. Miniaturised channels may also result in an accelerated binding reaction and fast response. Therefore, the combination of microfluidic technologies and sensors offers significant advantages for improving the overall performance of sensing detection and opens up many possibilities for a broad range of fields, such as preclinical early diagnosis, high-throughput screening, and personal point-of-care tests.

Recently, several different kinds of inorganic particles-integrated microfluidic sensing systems have been developed and their advantages are obviously observed through real-time and trustworthy results. Among these studies, the *in situ* synthesis of gold or silver particles inside microfluidic channels and SERS-based sensing detection are extensively investigated. Generally, gold and silver particles can be specifically trapped [217] or deposited into microchannels with a controllable pattern, such as hexagonal array [227] and thin film [40]. Galvanic replacement of a pre-patterned copper substrate in a microfluidic channel is also commonly used to fabricate *in situ* SERS structures [54,58]. The Au/Ag-patterned channel can be directly implemented as a microfluidic SERS sensor for providing real-time detection of various analytes, such as Rhodamine 6G [217], benzenethiol [227], bovine somatotropin [39], glucose [52], arsenic(III) [52],

Table 4. Examples of hybrid micro-/nanocomposites synthesised in microfluidic devices.

Particle type	Microreactor type	Particle property	Reaction condition	Key precursors	Ref
Inorganic–inorganic composite (by particle type)					
Ag@Cu_2O	T/cross-shaped capillary reactor	~100 nm; triangle	0.25–0.5 mL min^{-1}	$CuSO_4$+NaOH + $AgNO_3$+ $NaBH_4$	2017[183]
Ag–ZnO	T/cross-shaped capillary reactor	~500 nm; hedgehog-like	R.T.; 1 mL min^{-1}	$AgNO_3$+Zn $(NO_3)_2$+$NaBH_4$+NaOH	2016[184]
Al_2O_3/SiO_2–Fe_3O_4	Droplet-based reactor	100–200 μm	R.T.; 0.5–28 mL h^{-1}	Al_2O_3/SiO_2+Fe_3O_4	2011[185]
AuPd	Interdigital multilaminar reactor; cyclone micromixer	0.9–2.8 nm	R.T.; 1.92–2.6 L h^{-1}	$HAuCl_4$+H_2PdCl_4/K_2PdCl_4	2014[78] 2018[79]
Au@Ag	Combinatorial capillary; CDrAG-based reactor	~16–100 nm; sphere, star-like	R.T.; 0.063–58.9 μL min^{-1}	$HAuCl_4$+$AgNO_3$	2007[186], 2013[80,81]
Au@Ag@Au	T-shaped mixer	46 nm	R.T.; 150–300 μL min^{-1}	$HAuCl_4$+$AgNO_3$	2011[187]
CdS@CdSe	Serpentine micromixer		R.T.; 4–16 μL min^{-1}	$CdCl_2$+Na_2S + Na_2Se	2004[116]
CdSe@ZnS	Y-type micromixer; capillary reactor	~2–5 nm	120–300°C; 100 μL min^{-1}	$Cd(OAc)_2$/CdO + Se + ZnS	2004[137], 2005[125], 2008[128]
CdTe@ZnS	Y-shaped reactor	~1.5–3 nm; Man-/Gal-capped	90–160°C; 33.33 μL min^{-1}	CdO + Se	2010[130]
$CePO_4$@CdTe	Capillary reactor	3–5 nm × 200–300 nm (rod)	130°C; 2.5–15 mL min^{-1}	$Cd(NO_3)_2$+NaHTe + $CeCl_3$+ NaH_2PO_4	2010[188]
CoSm	Y-shaped mixer	~5 nm	2–50°C; N_2	$CoCl_2$+$SmCl_3$	2009[88]
Co_3O_4@SiO_2	T-shaped mixer	~165 nm	R.T.; 24.3–194.4 μL min^{-1}	TEOS + CTAB + $Co(NO_3)_2$	2017[189]
Cu@Cu_2O	Multichannel tubular reactor	6–14 nm	R.T.; 0.1–40 mL min^{-1}	$CuSO_4$+$NaBH_4$+PVP	2015[95]
FeCo	Y-shaped mixer	<5 nm	0–90°C; 0.2–3 mL min^{-1}	$CoCl_2$+$FeCl_2$+$NaBH_4$	2014[97]
$FeGa_2O_4$	Pneumatic micromixer	157 nm; hollow	145°C; 50–300 μL min^{-1}	$FeCl_2$+GaOOH	2009[190]
FeMn	Y-shaped mixer	~5 nm	R.T.; 4–15 μL min^{-1}	$FeSO_4$+$MnCl_2{\cdot}4H_2O$	2012[98]
Fe_2O_3@SiO_2	T-shaped mixer	50 nm	R.T.; 50–200 μL min^{-1}	Fe_2O_3+TEOS	2009[99]
Fe_3O_4@SiO_2@Pt	T-shaped mixer	85 nm	160°C; 20–100 μL min^{-1}	Fe_3O_4+TEOS + K_2PtCl_4	2012[191]
Fe(B)@Fe_xO_y	Y-shaped mixer	~10–25 nm; 70–100 emu g^{-1}	60–90°C; N_2; 1 mL min^{-1}	$FeCl_2$+$NaBH_4$+PVP	2013[192]
GM-Fe_3O_4	Y-shaped mixer	19.7–25.5 μm	900°C; H_2; 1–75 μL min^{-1}	GO + Fe_3O_4	2013[193]
$LaF_3/LaPO_4$–Ce, Tb	Microwave-integrated reactor	4.5–70 nm; sphere, rod	110°C/microwave (20 s)	$Ln(NO_3)_3$+$NH_4F/NH_4H_2PO_4$	2010[194]
PtBi	Capillary reactor	4–33.5 nm; sphere, rod	200–350°C; N_2	$Bi(NO_3)_3$+H_2PtCl_6	2015[105]
Pt–MPS/TiO_2/MPT	Segmented flow reactor	3 nm	R.T.; N_2;	H_2PtCl_6+TEOS/TBT	2012[195]
SiO_2@Au	T-shaped mixer; interdigital micromixer	79–260 nm	R.T.–65°C; N_2/CO; 2–80 μL min^{-1}	TEOS + $HAuCl_4$	2010[196], 2012[22], 2013[197]
SiO_2@Au/Fe_2O_3	Y-shaped mixer	~200 nm	R.T.; 1–5 μL min^{-1}	SiO_2+Au/Fe_2O_3	2013[198]
SiO_2@TiO_2	T-shaped mixer; Droplet-based reactor	~260 nm–300 μm	R.T.; N_2; 50–800 μL min^{-1}	SNPs + TEOT/TBT	2007[199], 2011[200]
SiO_2–Fe_3O_4	Droplet-based reactor	150 μm	R.T.; 0.5–2 mL h^{-1}	SiO_2+Fe_3O_4+silicon oil	2013[201]
ZnS–Mn	T-shaped mixer	~3 nm; TG-capped	R.T. – 80°C	ZnS + Na_2S + $MnCl_2$+TG	2008[202]
ZnS@CdSe@ZnS	Glass capillary reactor	5.5 nm	150–240°C; 10 μL min^{-1}	$Cd(OAc)_2$+Se	2009[141]
ZnSe@ZnS	Serpentine micromixer	3–4 nm	220°C; 5–30 μL min^{-1}	$Zn(OAc)_2$+Se	2012[144]
Inorganic–organic composite (by particle type)					
Ag-Chitosan	Droplet-based reactor	~300–600 μm	R.T.; 0.02–0.16 mL h^{-1}	$AgNO_3$+chitosan + $NaBH_4$	2016[203]
Ag-polyacrylamide	Droplet-based reactor	350 μm	R.T.; 20–150 μL min^{-1}	$AgNO_3$+$NaBH_4$+acrylamide	2013[55]
Ag/ZnO@PMMA	Segmented flow reactor	0.25 × 25 μm (rod); 3–4 μm (flower)	R.T.–160°C; 80–5000 μL min^{-1}	$AgNO_3/Zn(Ac)_2$+PMMA	2013[112]
Au/FeO/QD-μHDL	Straight 3-inlet reactor	8.1–30 nm	R.T.; 1–5 mL min^{-1}	Au/FeO/QD + MHPC + apoA	2013[204]
Au/ZnO–PTPGDA	T-shaped mixer	~25–65 μm	R.T.; 0.4–180 μL min^{-1}	$HAuCl_4$+$Zn(OAc)_2$+TPGDA	2010[205]
Au–PEO-*b*–PS	Straight 3-inlet reactor	100–600 nm	R.T.; 5–90 μL min^{-1}	$HAuCl_4$+PEO-*b*-PS	2013[206]
Au–PS	Segmented flow reactor	~1 mm × ~4 mm (rod)	80°C	$HAuCl_4$+styrene + DVB	2007[207]

(*Continued*)

Table 4. Continued.

Particle type	Microreactor type	Particle property	Reaction condition	Key precursors	Ref
$BaSO_4$–PNIPAM	Droplet-based reactor	~40 μm	R.T.; 20–180 μL h^{-1}	$BaCl_2$+$(NH_4)_2S_2O_8$+NIPAM	2013[208]
CdS–PS-*b*–PAA	Segmented flow reactor	40–140 nm	R.T.; 0.4–28.9 μL min^{-1}	CdS + styrene + AA	2008[209], 2010[210]
CdSe@ZnS–HFR	Serpentine micromixer	130 nm	R.T.	CdSe@ZnS + heparin + FA + RA	2012[211]
CdSe@ZnS–PLGA	Droplet-based reactor	180–550 μm	R.T.; 0.02–1 mL min^{-1}	CdO + Se + $ZnMe_2$+$S(SiMe_3)_2$	2007[212]
CdSe@ZnS-lipid-PLGA	Droplet-based reactor	60 nm	R.T.; 50 μL min^{-1}	CdSe@ZnS + PLGA + DPSE	2010[213]
CdSe@ZnS–ETPTA–PEG	Droplet-based reactor	~50–200 μm	R.T.; 1–8 mL h^{-1}	CdSe@ZnS + ETPTA + PEG	2011[214], 2014[215]
CdSe@ZnS/Fe_2O_3-PEG-*b*-PLA	Droplet-based reactor	~75 μm	R.T.; 1–400 μL min^{-1}	CdSe@ZnS/Fe_2O_3+PEG-*b*-PLA	2012[216]
Chitosan@Au	T-shaped mixer	~120 μm	R.T.; 500 μL h^{-1}	$HAuCl_4$+chitosan	2010[217]
Chitosan@TS-1/Fe_3O_4/TiO_2	Droplet-based reactor	200–600 μm	R.T.; 20 μL min^{-1}	Chitosan + TS-1/Fe_3O_4/TiO_2	2011[218]
Fe_2O_3-hydrogel	T-shaped mixer	~30–40 μm; sphere, disk, plug	R.T.; 5.5–62.7 kPa	$FeCl_3$+$FeCl_2$+PEGDA	2008[219]
Fe_2O_3–PLGA	Cross-channel reactor	~110 nm	R.T.; 0.3–2 (flow ratio)	$FeCl_3$+$FeCl_2$+PLGA	2015[220]
Fe_3O_4–alginate	Laminar flow reactor	211–364 μm (diameter); fibre	R.T.; 1–5 mL min^{-1}	Fe_3O_4+$CaCl_2$+$C_6H_9NaO_7$	2012[221]
Fe_3O_4/TiO_2–PMMA	T-shaped mixer	185 μm	R.T.; 0.05–0.1 mL min^{-1}	Fe_3O_4/TiO_2+MMA	2013[180]
MOF	Y-shaped mixer; T-shaped mixer	90 nm–150 μm; Angular, sphere, cube, rod	R.T.–160°C; 1–600 μL min^{-1}	$FeCl_3$/$Cu(NO_3)_2$/$Zn(NO_3)_2$/$ZrCl_4$/$RuCl_3$+H_2BDC/H_3BTC	2013 [222,223]
Pt–PVP–TMPTA	Droplet-based reactor	106 μm	R.T.; 0.8–4 mL h^{-1}	K_2PtCl_4+PVP + TMPTA	2016[224]
SiC–PFPE	Droplet-based reactor	162 μm	R.T.; 5 μL min^{-1}	AHPCS + PFPE	2009[225]
SiO_2-Chitosan	Droplet-based reactor	250 μm	R.T.; 10–300 μL min^{-1}	TEOS + chitosan	2010[226]
SiO_2-ETPTA@Ag	Droplet-based reactor	77 μm	R.T.	SiO_2-ETPTA + $AgNO_3$	2011[227]
SiO_2-hydrogel	Droplet-based reactor	110 μm (Janus sphere); 115μm × 58 μm (Janus discoid)	R.T.; 100 μL h^{-1}	SNPs + Acrylamide	2006[179]
SiO_2–PS-*co*–PAA	T-shaped mixer	~100 μm	R.T.; CO_2; 7.5–24 mL h^{-1}	TEOS + styrene + AA	2009[228]
SiO_2-lipid	Droplet-based reactor	3–16 μm	R.T.; 5–22 psi; 1–7 mL h^{-1}	TEOS + PFB + DPPC + DPPE	2010[229], 2013[230]
SiO_2-TS-1/PS	Droplet-based reactor	200–600 μm	R.T.; 10–40 μL min^{-1}	SiO_2+TS-1/PS	2012[231]
SiO_2@Dextran	Droplet-based reactor	150–400 nm	R.T.; 3 mL h^{-1}	SiO_2+Dextran	2015[232]
YVO_4-Eu/Dy/Sm-PEG–PAA	Herringbone mixer	46.4 μm	R.T.	YVO_4-Eu/Dy/Sm + PEG + PAA	2012[233]

Abbreviations: AA: acrylic acid; AHPCS: allylhydridopolycarbosilane; CDrAG: concentration-gradient droplet array generator; DPPC: 1,2-dipalmitoyl-sn-glycero-3-phosphocholine; DPPE: 1,2-dipalmitoyl-sn-glycero-3-phosphoethanolamine; DVB: divinyl benzene; ETPTA: ethoxylated trimethylolpropane triacrylate; FA: folic acid; GM: graphite microball; GO: graphene oxide; HDL: high-density lipoprotein; HFR: heparin-folic acid-retinoic acid; MHPC: 1-myristoyl-2-hydroxy-sn-glycero-3-phosphocholine; MMA: methyl methacrylate; MOF: metal–organic framework; MPS: mesoporous silica; MPT: mesoporous titania; NIPAM: *N*-isopropylacrylamide; PAA: poly(acrylic acid); PEGDA: poly(ethylene glycol) diacrylate; PEO: poly(ethylene oxide); PFB: perfluorobutane; PFPE: perfluoropolyether; PLGA: poly(DL-lactide-*co*-glycolide); PMMA: poly(methyl methacrylate); PNIPAM: poly(*N*-isopropylacrylamide); PS: polystyrene; PTPGDA: poly(tri(propylene glycol) diacrylate); PVP: poly(vinylpyrrolidinone); RA: retinoic acid; SNPs: silica nanoparticles; TBT: tetrabutyl titanate; TEOS: tetraethylorthosilicate; TEOT: titanium tetraethoxide; TG: 1-thioglycerol; TMPTA: trimethylolpropane triacrylate; TPGDA: tri(propylene glycol) diacrylate; TS-1: titanium silicate molecular sieve.

hydrogen peroxide [37], crystal violet [54], adenosine [40], pesticides, and herbicides [58]. The Au/Ag-patterned microchannel can be further modified with specific antibody to realise ultrasensitive detection of antigen (Figure 7(A)) [39]. Due to its limited space and enhanced mixing efficiency, this kind of integrated microfluidic sensor could significantly reduce the using amount of expensive antibodies while improving the overall sensing performance, such as stability, specificity, reproducibility, and sensitivity. Except for SERS-based sensing detection, the Au/Ag-patterned microchannel can be also used for on-chip electrochemical detection (Figure 7(B)). The continuous streaming solution in microfluidic device allows for enhanced mass transport to the integrated electrodes and elimination of fouling effects, resulting in increased currents and high sensitivity [52]. Therefore, the current response will show good linearity in a wide concentration range of analytes and remarkable sensitivity in a short response time. In addition to the *in situ* microfluidic sensing systems, Au/Ag-containing composites produced via microfluidic devices can be applied for single particle-based SERS microsensor (Figure 7(C)). Swellable polymer composites having a high content of Au/Ag nanoparticles are of great interest for SERS-based analytical measurements. This technique permits a significant increase in the sensitivity of vibration spectrometry by several orders of magnitude [55].

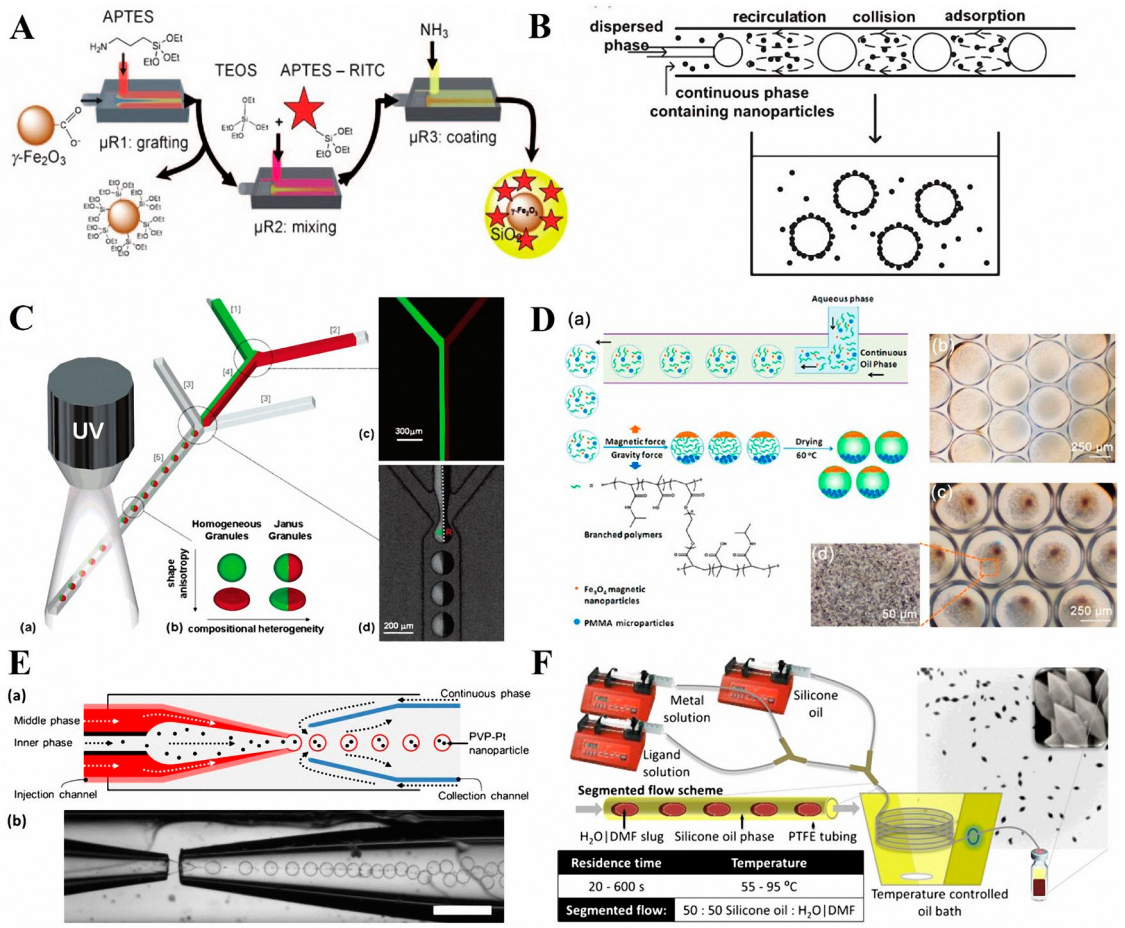

Figure 6. Microfluidic systems for hybrid micro-/nanoparticles synthesis. (A) Scheme for the continuous synthesis of fluorescent core/shell magnetic/silica nanoparticles. μR1: microreactor for grafting APTES onto the citrated γ-Fe_2O_3 nanoparticles; μR2: microreactor for mixing of the sol–gel precursors TEOS and APTES-RITC; μR3: microreactor for coating of the γ-Fe_2O_3 nanoparticles with silica [99]. (B) Controllable preparation of TS-1 nanoparticle-coated chitosan microspheres in a co-axial microfluidic device [218]. (C) Microfluidic assembly of homogeneous and Janus colloid-filled hydrogel granules [234]. (D) Multicompartmental Janus microbeads from branched polymers by single-emulsion droplet microfluidics [235]. (E) Microfluidic encapsulation of polyvinylpyrrolidone (PVP)-Pt nanoparticles in microcapsules [224]. (F) Schematic of the microfluidic setup, segmented flow pattern, and synthesis details for accelerating the synthesis of metal–organic frameworks [222]. All images reproduced with permission.

Molecular catalysis for microreactions

One of the drawbacks of conventional batch methods to synthesise metallic catalysts is the lack of suitable control over mixing. Poor mixing leads to catalysts with wide size distribution, irreproducibility structure and surface, and hard to scale-up. Microfluidic synthesis techniques permit superior control over reaction conditions and allow more efficient heat and mass transfer. These advantages are key for producing a wide range of catalysts with minimum reaction time, high yields, and more uniform structural properties. In this context, various catalytic applications of those metallic particles and their composites from microreactors are being explored.

Microfluidic flow synthesis could yield metallic catalysts with desired size, shape, and crystallinity that are not easily achieved by conventional batch methods. The recent study showed that even subnanometer gold particles with high monodispersity can be successfully synthesised using a micromixer (Figure 8(A)). Comparison test further revealed that microfluidic synthesis could produce smaller-sized monodisperse gold particles than batch synthesis method, and microfluidics-generated catalysts exhibited higher catalytic activity for the aerobic oxidation of *p*-hydroxybenzyl alcohol than batch-prepared gold catalysts (Figure 8 (A)) [30]. The as-synthesised metallic catalysts can be also incorporated onto the inner surface (2D dispersion) or into the inner volume (3D dispersion) of functionalised microfluidic channels to build catalytic microreactors dedicated to fine chemical reactions [49]. Thin films of mesoporous silica, titania, or mesoporous titania can be provided as support layers to enhance the adsorption and catalytic activity of metallic catalysts inside the microreactor [195]. Using such immobilisation method, example showed that Pt nanoparticles inside the microreactor exhibited superior catalytic activity for the hydrogenation of nitrobenzene to aniline and were easily regenerated even after they were deactivated (Figure 8(B)) [195].

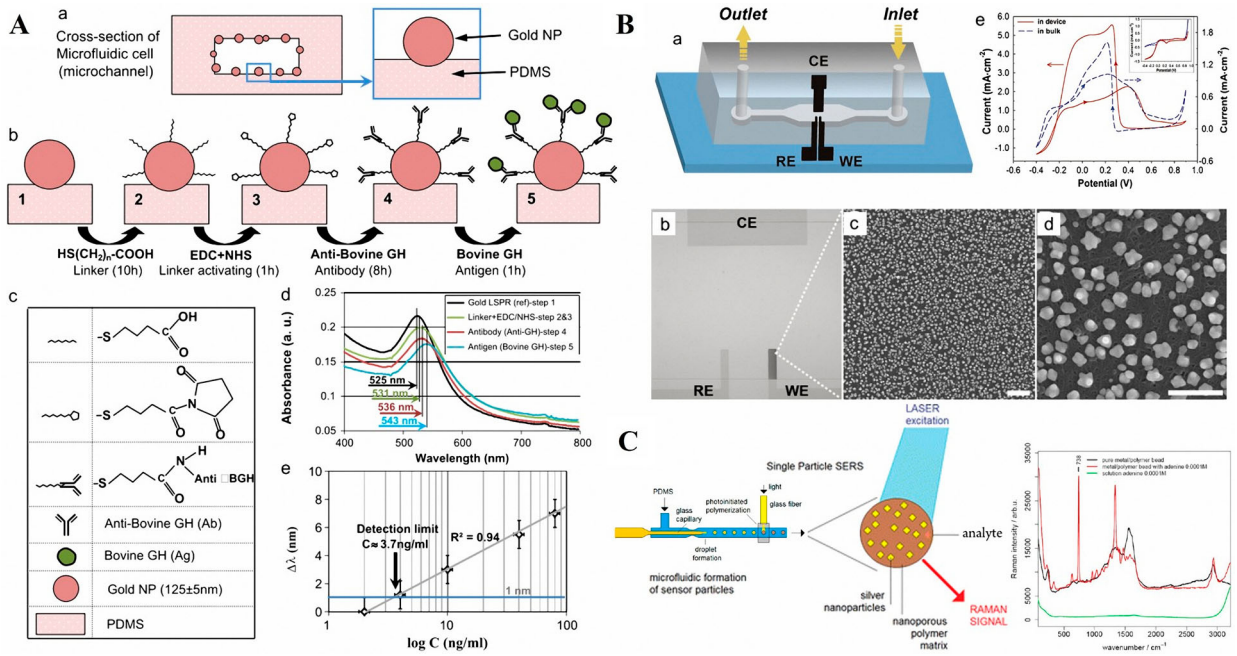

Figure 7. Applications of microfluidics-based inorganic particles in biosensing and in vitro detection. (A) Biosensing experiments performed using the annealed microfluidic biosensor prepared from 2% aqueous solution of the gold precursor (48 h) [39]. (B) On-chip electrochemical detection of glucose by Au nanostructures fabricated in a microfluidic channel [52]. (C) Polyacrylamid/silver composite particles produced via microfluidic photopolymerisation for single particle-based SERS microsensorics [55]. All images reproduced with permission.

In addition, microfluidic techniques can be used to produce various inorganic–organic and inorganic–inorganic hybrid composites with promising catalytic activities [78,95,105,191,223,224]. For example, compared to quasi-homogeneous catalysis of Pt nanoparticles for 4-nitrophenol hydrogenation, the encapsulated Pt catalysts inside microcapsules display excellent catalytic activity, a leaching-proof nature, and high reusability under the same reaction conditions (Figure 8(C)) [224]. Similarly, the highly monodisperse binary metallic composites produced from microreactors exhibited obviously enhanced catalytic activities because of synergistic effects (Figure 8(D)) [78]. Furthermore, hierarchical catalyst composites consisting of metal decorated iron oxide structure can be yielded by a successive microfluidic approach and be easily immobilised into microreactor for achieving excellent catalytic activity (Figure 8(E,F)). It is also noting that, after the reactions, all the hierarchical catalysts can be recovered using the magnetic property of the underlying iron oxide particles [191,223].

Bioimaging, drug delivery, and tumour targeting

The development of new and improved particle-based biomedicine systems is underpinned by an enhanced ability to engineer particles with optimised physicochemical properties, as well as increased knowledge of their biological performance. Microfluidic techniques can greatly facilitate these processes through controlled microenvironments with high spatiotemporal resolution. Specifically, miniaturised reactor platforms provide controlled laminar fluid transport, rapid chemical reactions, and cost-saving advantages over conventional batch methods for biomedicine-related applications, especially for high-throughput drug screening [236], drug delivery [9,237–239], theranostics [240], tissue engineering [8], and cancer treatment [5].

Most of the current inorganic particles-based biomedicine systems were established in combination with organic components because of the synergistic potential for bioactivity, structural biocompatibility, and multifunctionality. In bioimaging, microfluidics-based manufacturing methods can integrate proteins or polymers with gold or $BaSO_4$, iron oxide, and QDs, which enable the recognition of biological samples by X-ray computed tomography, magnetic resonance imaging, and fluorescent microscopy, respectively (Figure 9(A)) [204,208]. In antibacterial field, microfluidics permits to fabricate uniform and monodisperse bactericidal composites, such as Ag-loaded chitosan microparticles. Their size and content can be easily tuned by adjusting the flow rate and precursor concentration, respectively. These advantages enable to significantly enhance the antibacterial capability because of the synergistic effect between inorganic component (e.g. Ag) and organic component (e.g. Chitosan) (Figure 9(B)) [203]. Drug delivery is another promising field that can be exploited with well-defined inorganic–organic composites produced from microreactors. In recent years, microfluidic techniques have already been successfully used to

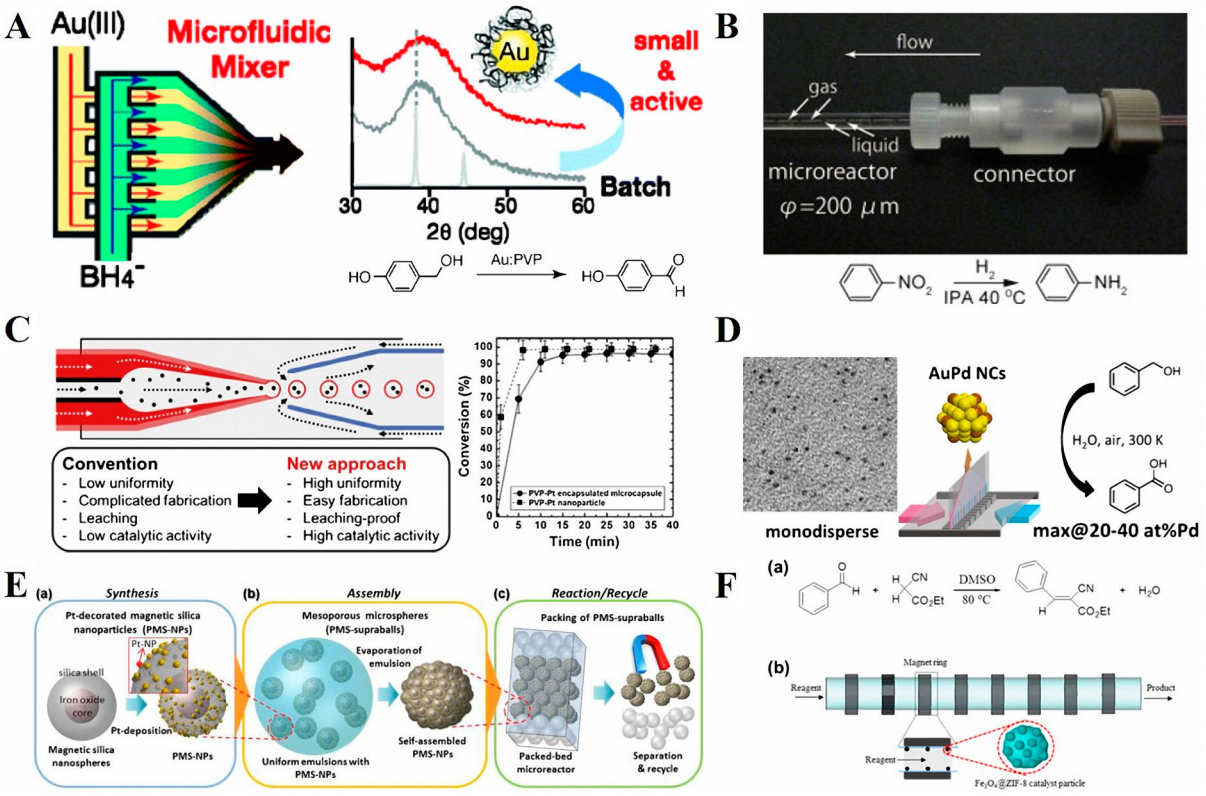

Figure 8. Applications of microfluidics-based inorganic particles in catalysis. (A) Microfluidic synthesis of PVP-stabilised, ~1 nm gold clusters that exhibited higher catalytic activity for the aerobic oxidation of *p*-hydroxybenzyl alcohol than did Au:PVP clusters prepared by batch methods [30]. (B) Pt nanoparticles were immobilised inside a microreactor to catalyse the hydrogenation of nitrobenzene to aniline [195]. (C) Microfluidic preparation of a highly active and stable catalyst for 4-nitrophenol hydrogenation by high performance of encapsulation of polyvinylpyrrolidone (PVP)-Pt nanoparticles in microcapsules [224]. (D) Development of ultrafine multichannel microfluidic mixer for synthesis of bimetallic nanoclusters: application of highly monodisperse AuPd nanoclusters for catalytic aerobic oxidation of benzyl alcohol [78]. (E) Schematic illustration of the use of multiple microfluidic systems in the synthesis, self-assembly, and catalysis with Pt-decorated magnetic silica (PMS) supraballs [224]. (F) Microfluidic approach towards continuous and ultrafast synthesis of metal–organic framework crystals and hetero structures in confined microdroplets for Knoevenagel condensation [223]. All images reproduced with permission.

engineer stable drug carriers with monodisperse size, excellent biocompatibility, and controllable release profiles, which are major challenges faced by conventional drug delivery systems. Regardless of the solubility of the drugs, microreactors can encapsulate them inside different kinds of micro-/nanocomposites [221,230,232], and multiple drugs with different physicochemical properties can be simultaneously loaded into the composites with a desired ratiometric control [232]. The drug carriers can be also assembled as a stimuli-responsive system for realising controllable release kinetics under external stimuli, such as pH [230] or magnetic force (Figure 9(C,D)) [221]. To achieve the targeted drug delivery, more advanced drug carriers conjugated with targeting ligands can be also efficiently fabricated through microfluidic self-assembly approach [232]. In addition, results showed that, compared with the conventional batch methods, microfluidic techniques can produce smaller and more compact drug carrier composites with narrower size distribution and higher drug loading amount [220]. In vivo study further verified that bone-targeting microfluidic drug delivery composites behaved more prolonged circulation and higher tumour localisation and suppression towards bone metastatic tumour than their conventional counterparts (Figure 9(D)).

Conclusions, current challenges, and future perspectives

The field of microfluidic synthesis and applications of inorganic micro-/nanoparticles has already demonstrated a great deal of potential. Compared to conventional batch methods relying on bulk mixing that largely tend to suffer from difficulties to implement fast screening of particle properties and poor reproducibility from batch to batch, microfluidics-based flow synthesis has shown the capability to produce micro-/nanoparticles in a controllable and reproducible manner, offering excellent performance for many biomedical applications, such as biosensing, molecular catalysis, and biomedicine. The successful synthesis and applications of microfluidics-based inorganic micro-/nanoparticles can be summarised mainly as follows. (1) The rapid and sufficient mixing in microfluidic channels induced by hydrodynamic focusing results

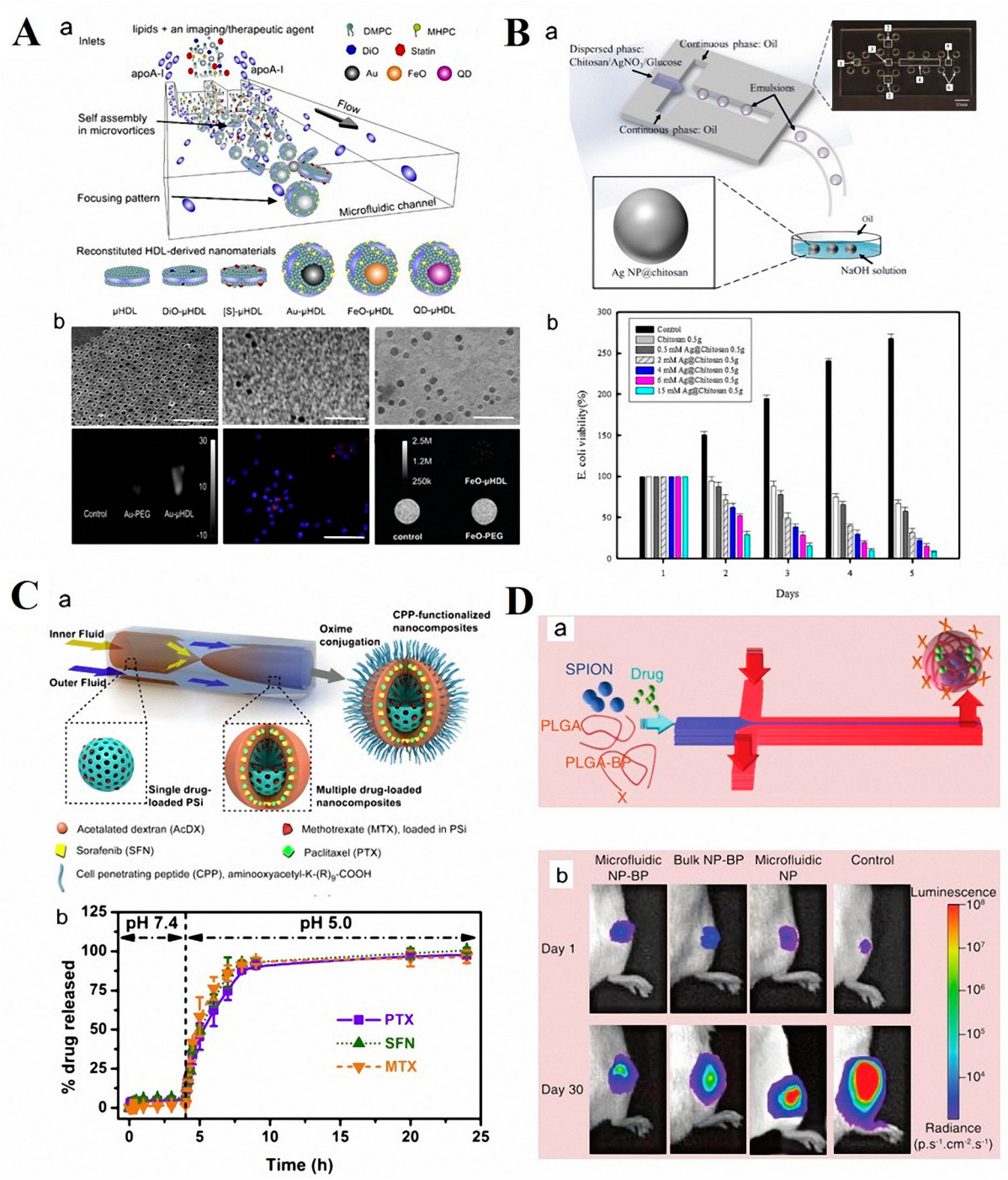

Figure 9. Applications of microfluidics-based inorganic particles in biomedicine. (A) Microfluidic reconstitution of HDL-derived nanomaterials (μHDL) for bioimaging. (a) A schematic depiction of a microfluidic platform that allows single-step and large-scale production of the HDL; (b) Au-μHDL for CT imaging (left panel), QD-μHDL for fluorescence (middle panel), FeO-μHDL for MRI (right panel) [204]. (B) Microfluidic assisted synthesis of silver nanoparticle–chitosan composite microparticles for antibacterial applications [203]. (C) Microfluidic assisted one-step fabrication of porous silicon@acetalated dextran nanocomposites for precisely controlled drug delivery [232]. (D) On-chip synthesis of fine-tuned bone-seeking hybrid nanoparticles. (a) Schematic representation of the cross-junction microfluidic device used for controlled formation of PLGA-based (magnetic/targeted) NPs. (b) Bioluminescence images of mice after injection of luciferase-positive human breast cancer cells (MDA-MB-231) in tibia of BALB/c mice at day 1 and 30 [220]. All images reproduced with permission.

in uniform and monodisperse particles with a relatively high yield. (2) The precise and accurate control over synthetic conditions enables fine modulation of the physicochemical properties and small batch-to-batch variation. (3) The systematic integration of multiple synthetic procedures into a single microfluidic device allows for the generation of micro-/nanoparticles with desired complex structures and unique multifunction in one step. (4) Microreactor technology provides enhanced process control based on well-defined microstructures of the active unit cell that can be replicated to yield higher chemical production volumes. These

specific features make the microfluidic device an ideal system for controllable synthesis and practical applications of inorganic micro-/nanoparticles.

Despite the recent advances on the synthesis of different categories of inorganic particles (including metals, metal oxides, metal salts, QDs, silica, and hybrid composites) and their applications in several different fields (including biosensor, molecular catalysis, and biomedicine), the synthesis and applications of microfluidics-based inorganic particles are still at their early stages. Many aspects need to be carefully considered and addressed to advance this technology. These challenges include, but not limited to, (1) the scalability of the production rate. Due to the small dimensions of the operating microchannels and the increased pressure drop with increasing flow rate, the current maximum mass production rate was around gram-scale per hour [34,122]. To realise the particle productions on an industrial level, new and robust designs of microfluidic devices with stacked microreactor system and industrial-scale fluid control apparatus need to be considered to realise scalable manufacturing and achieve kilograms-scale or even higher per hour. (2) The regulation of particle shapes. Of the different types of particles investigated to date, the size, composition, and surface chemistry properties have been studied in great detail. But a majority of micro-/nanoparticles synthesised from microreactors are those of spherical shape. Since the shapes of particles could generate significant effects on their performance [241–245], more efforts should be devoted to the synthesis of anisotropic particles. For example, in our recent studies, by adopting self-templating and flow rates manipulation methods, hollow ellipsoid-like and fibre-like mesoporous silica materials can be produced in a controllable way [179,181]. (3) The integration of inline measurement systems. Inline measurement systems provide a real-time information of as-synthesised particles and an immediate feedback control, reducing the time needed during the screening and optimisation processes. However, despite the appealing features of inline measurement systems, only limited studies have been devoted to this area. (4) The mechanisms of inorganic micro-/nanoparticles synthesis at multiple scale. The optimal design for the microfluidic synthesis of particles requires a full and deep understanding of the underlying governing principles. Such information obtained from using either microreactors or conventional batch methods is still incomplete; we anticipate thorough investigations into unravelling the underlying principles, facilitated by the microreactors technologies. (5) The evaluation matrix of microfluidics-based particles. Investigations towards this direction have been recently published with promising results, but there are still limited studies on the direct comparison of particles' performance between microfluidic approach and conventional batch approach [30,220,224]. (6) The transition from bench-side prototypes to industry. As noted above, an extensive assessment on a range of chemical reactions performed in microreactor and batch reactor concludes that there are usually a remarkable decrease in the reaction residence time and an increase in selectivity and conversion yield in microreactors. Owing to their cost advantages and sustainability, such green chemistry and engineering approaches are attractive to industry. In recent years, some companies such as Lonza, Corning, and Syrris have conducted pioneering research to produce robust and flexible microreactors with industrial-level capacities [246], which provide useful guide to the development of microfluidic technology for industrial environment. (7) The clinical translation of micro-/nanoparticles. Although the field of microfluidics applied into biomedical engineering is still in its infancy, microfluidic technologies can be adopted as an efficient tool to identify optimal particles and undoubtedly capable of accelerating their translation. It is anticipated that, among all the microfluidic technologies, those developed for the chemical synthesis and in vitro/in vivo screening of micro-/nanoparticles have the highest probability of generating an impact in the near future.

Nevertheless, despite of the fact that the use of microfluidic devices for micro-/nanoparticles synthesis is still under intensive exploration, research carried out in the last two decades especially in the last five years has demonstrated that microfluidics could facilitate the synthesis of micro-/nanoparticles for a variety of new promising applications. Given new advancements that are occurring in both microfluidic technologies and micro-/nanomaterials designs, the expansion of the knowledge at their intersection will inevitably provide new insights in the near future for producing functional materials applicable in biomedical engineering.

Disclosure statement

No potential conflict of interest was reported by the authors.

Funding

The authors are grateful for the financial support from the National Institute of Health (NIH) Director's Transformative Research Award (R01HL137157), National Science Foundation (NSF) ECCS-1509369, 1128677 and 1309686, and Norris Cotton Cancer Center Developmental Funds (Pilot Projects).

References

[1] Hao NJ, Li LF, Tang FQ. Roles of particle size, shape and surface chemistry of mesoporous silica

nanomaterials on biological systems. Int Mater Rev. 2017;62:57–77.
[2] Hao NJ, Neranon K, Ramström O, et al. Glyconanomaterials for biosensing applications. Biosens Bioelectron. 2016;76:113–130.
[3] Alaca B E. Integration of one-dimensional nanostructures with microsystems: an overview. Int Mater Rev. 2009;54:245–282.
[4] Marre S, Jensen KF. Synthesis of micro and nanostructures in microfluidic systems. Chem Soc Rev. 2010;39:1183–1202.
[5] Feng Q, Sun J, Jiang X. Microfluidics-mediated assembly of functional nanoparticles for cancer-related pharmaceutical applications. Nanoscale. 2016;8:12430–12443.
[6] Zhao C-X, He L, Qiao SZ, et al. Nanoparticle synthesis in microreactors. Chem Eng Sci. 2011;66:1463–1479.
[7] Dendukuri D, Doyle PS. The synthesis and assembly of polymeric microparticles using microfluidic. Adv Mater. 2009;21:4071–4086.
[8] Chung BG, Lee K-H, Khademhosseini A, et al. Microfluidic fabrication of microengineered hydrogels and their application in tissue engineering. Lab Chip. 2012;12:45–59.
[9] Capretto L, Carugo D, Mazzitelli S, et al. Microfluidic and lab-on-a-chip preparation routes for organic nanoparticles and vesicular systems for nanomedicine applications. Adv Drug Deliv Rev. 2013;65:1496–1532.
[10] Wang W, Zhang M-J, Chu L-Y. Functional polymeric microparticles engineered from controllable microfluidic emulsions. Acc Chem Res. 2014;47:373–384.
[11] Baah D, Floyd-Smith T. Microfluidics for particle synthesis from photocrosslinkable materials. Microfluid Nanofluid. 2014;17:431–455.
[12] Hao NJ, Zhang XJ. Microfluidic screening of circulating tumor biomarkers towards liquid biopsy. Sep Purif Rev. 2018;47:19–48.
[13] Sackmann EK, Fulton AL, Beebe DJ. The present and future role of microfluidics in biomedical research. Nature. 2014;507:181–189.
[14] Abou-Hassan A, Sandre O, Cabuil V. Microfluidics in inorganic chemistry. Angew Chem Int Ed. 2010;49:6268–6286.
[15] Song Y, Hormes J, Kumar CSSR. Microfluidic synthesis of nanomaterials. Small. 2008;4:698–711.
[16] Luo G, Du L, Wang Y, et al. Controllable preparation of particles with microfluidics. Particuology. 2011;9:545–558.
[17] Teh S-Y, Lin R, Hung L-H, et al. Droplet microfluidics. Lab Chip. 2008;8:198–220.
[18] Lin XZ, Terepka AD, Yang H. Synthesis of silver nanoparticles in a continuous flow tubular microreactor. Nano Lett. 2004;4:2227–2232.
[19] Uson L, Sebastian V, Arruebo M, et al. Continuous microfluidic synthesis and functionalization of gold nanorods. Chem Eng J. 2016;285:286–292.
[20] Boken J, Soni SK, Kumar D. Microfluidic synthesis of nanoparticles and their biosensing applications. Crit Rev Anal Chem. 2016;46:538–561.
[21] Chan EM, Alivisatos AP, Mathies RA. High-temperature microfluidic synthesis of CdSe nanocrystals in nanoliter droplets. J Am Chem Soc. 2005;127:13854–13861.
[22] Gomez L, Arruebo M, Sebastian V, et al. Facile synthesis of SiO2–Au nanoshells in a three-stage microfluidic system. J Mater Chem. 2012;22:21420–21425.
[23] Kashid MN, Gupta A, Renken A, et al. Numbering-up and mass transfer studies of liquid-liquid two-phase microstructured reactors. Chem Eng J. 2010;158:233–240.
[24] Al-Rawashdeh M, Yu F, Nijhuis TA, et al. Numbered-up gas-liquid micro/milli channels reactor with modular flow distributor. Chem Eng J. 2012;207–208:645–655.
[25] Song H, Chen DL, Ismagilov RF. Reactions in droplets in microfluidic channels. Angew Chem Int Ed. 2006;45:7336–7356.
[26] Ma J, Lee S, Yi C, et al. Controllable synthesis of functional nanoparticles by microfluidic platforms for biomedical applications – a review. Lab Chip. 2017;17:209–226.
[27] Cabeza VS, Kuhn S, Kulkarni A, et al. Size-controlled flow synthesis of gold nanoparticles using a segmented flow micro fluidic platform. Langmuir. 2012;28:7007–7013.
[28] Duraiswamy S, Khan SA. Droplet-based microfluidic synthesis of anisotropic metal nanocrystals. Small. 2009;5:2828–2834.
[29] Wagner J, Tshikhudo TR, Köhler JM. Microfluidic generation of metal nanoparticles by borohydride reduction. Chem Eng J. 2008;135:S104–S109.
[30] Tsunoyama H, Ichikuni N, Tsukuda T. Microfluidic synthesis and catalytic application of pvp-stabilized, ~1 nm gold clusters. Langmuir. 2008;24:11327–11330.
[31] Shalom D, Wootton RCR, Winkle RF, et al. Synthesis of thiol functionalized gold nanoparticles using a continuous flow microfluidic reactor. Mater Lett. 2007;61:1146–1150.
[32] Lazarus LL, Yang AS-J, Chu S, et al. Flow-focused synthesis of monodisperse gold nanoparticles using ionic liquids on a microfluidic platform. Lab Chip. 2010;10:3377–3379.
[33] Boleininger J, Kurz A, Reuss V, et al. Microfluidic continuous flow synthesis of rod-shaped gold and silver nanocrystals. Phys Chem Chem Phys. 2006;8:3824–3827.
[34] Lohse SE, Eller JR, Sivapalan ST, et al. A simple millifluidic benchtop reactor system for the high-throughput synthesis and functionalization of gold nanoparticles with different sizes and shapes. ACS Nano. 2013;7:4135–4150.
[35] Weng C, Huang C, Yeh C, et al. Synthesis of hexagonal gold nanoparticles using a microfluidic reaction system. J Micromech Microeng. 2008;18:035019.
[36] Gomez L, Sebastian V, Irusta S, et al. Scaled-up production of plasmonic nanoparticles using microfluidics: from metal precursors to functionalized and sterilized nanoparticles. Lab Chip. 2014;14:325–332.
[37] Wang L, Ma S, Yang B, et al. Morphology-controlled synthesis of Ag nanoparticle decorated poly (o-phenylenediamine) using microfluidics and its application for hydrogen peroxide detection. Chem Eng J. 2015;268:102–108.
[38] Wagner J, Köhler JM. Continuous synthesis of gold nanoparticles in a microreactor. Nano Lett. 2005;5:685–691.
[39] SadAbadi H, Badilescu S, Packirisamy M, et al. Integration of gold nanoparticles in PDMS microfluidics for lab-on-a-chip plasmonic biosensing of

growth hormones. Biosens Bioelectron. 2013;44:77–84.
[40] Leem J, Kang HW, Ko SH, et al. Controllable Ag nanostructure patterning in a microfluidic channel for real-time SERS systems. Nanoscale. 2014;6:2895–2901.
[41] He S, Kohira T, Uehara M, et al. Effects of interior wall on continuous fabrication of silver nanoparticles in microcapillary reactor. Chem Lett. 2005;34:748–749.
[42] He ST, Liu YL, Maeda H. Controlled synthesis of colloidal silver nanoparticles in capillary micro-flow reactor. J Nanopart Res. 2008;10:209–215.
[43] Singh A, Shirolkar M, Lalla NP, et al. Room temperature, water-based, microreactor synthesis of gold and silver nanoparticles. Int J Nanotechnol. 2009;6:541–551.
[44] Sugano K, Uchida Y, Ichihashi O, et al. Mixing speed-controlled gold nanoparticle synthesis with pulsed mixing microfluidic system. Microfluid Nanofluid. 2010;9:1165–1174.
[45] Yang S-Y, Cheng F-Y, Yeh C-S, et al. Size-controlled synthesis of gold nanoparticles using a micro-mixing system. Microfluid Nanofluid. 2010;8:303–311.
[46] Gómez-de Pedro S, Puyol M, Alonso-Chamarro J. Continuous flow synthesis of nanoparticles using ceramic microfluidic devices. Nanotechnology. 2010;21:415603.
[47] Lee KG, Hong J, Wang KW, et al. In vitro biosynthesis of metal nanoparticles in microdroplets. ACS Nano. 2012;6:6998–7008.
[48] Lazarus LL, Riche CT, Marin BC, et al. Two-phase microfluidic droplet flows of ionic liquids for the synthesis of gold and silver nanoparticles. ACS Appl Mater Interfaces. 2012;4:3077–3083.
[49] Jamal F, Jean-Sébastien G, Maël P, et al. Gold nanoparticle synthesis in microfluidic systems and immobilisation in microreactors designed for the catalysis of fine organic reactions. Microsyst Technol. 2012;18:151–158.
[50] Liu H, Huang J, Sun D, et al. Microfluidic biosynthesis of silver nanoparticles: effect of process parameters on size distribution. Chem Eng J. 2012;209:568–576.
[51] Kumar D V. R, Prasad BL V, Kulkarni AA. Segmented flow synthesis of Ag nanoparticles in spiral microreactor: role of continuous and dispersed phase. Chem Eng J. 2012;192:357–368.
[52] Han KN, Li CA, Bui MPN, et al. On-chip electrochemical detection of bio/chemical molecule by nanostructures fabricated in a microfluidic channel. Sensor Actuat B. 2013;177:472–477.
[53] Horikoshi S, Sumi T, Serpone N. A hybrid microreactor/microwave high-pressure flow system of a novel concept design and its application to the synthesis of silver nanoparticles. Chem Eng Process. 2013;73:59–66.
[54] Parisi J, Su L, Lei Y. In situ synthesis of silver nanoparticle decorated vertical nanowalls in a microfluidic device for ultrasensitive in-channel SERS sensing. Lab Chip. 2013;13:1501–1508.
[55] Köhler JM, März A, Popp J, et al. Polyacrylamid/silver composite particles produced via microfluidic photopolymerization for single particle-based SERS microsensorics. Anal Chem. 2013;85:313–318.
[56] López-Lorente ÁI, Valcárcel M, Mizaikoff B. Continuous flow synthesis and characterization of tailor-made bare gold nanoparticles for use in SERS. Microchim Acta. 2014;181:1101–1108.
[57] Fu Q, Sheng Y, Tang H, et al. Growth mechanism deconvolution of self-limiting supraparticles based on microfluidic system. ACS Nano. 2015;9:172–179.
[58] Parisi J, Dong Q, Lei Y. In situ microfluidic fabrication of SERS nanostructures for highly sensitive fingerprint microfluidic-SERS sensing. RSC Adv. 2015;5:14081–14089.
[59] Hafermann L, Michael Köhler J. Small gold nanoparticles formed by rapid photochemical flow-through synthesis using microfluid segment technique. J Nanopart Res. 2015;17:152.
[60] Xu L, Peng J, Yan M, et al. Droplet synthesis of silver nanoparticles by a microfluidic device. Chem Eng Process. 2016;102:186–193.
[61] Kim DJ, Ha D, Zhou Q, et al. A cracking-assisted micro-/nanofluidic fabrication platform for silver nanobelt arrays and nanosensors. Nanoscale. 2017;9:9622–9630.
[62] Yagyu H, Tanabe Y, Takano S, et al. Continuous flow synthesis of monodisperse gold nanoparticles by liquid-phase reduction method on glass microfluidic device. Micro Nano Lett. 2017;12:536–539.
[63] Bandulasena MV, Vladisavljević GT, Odunmbaku OG, et al. Continuous synthesis of PVP stabilized biocompatible gold nanoparticles with a controlled size using a 3D glass capillary microfluidic device. Chem Eng Sci. 2017;171:233–243.
[64] Tofighi G, Lichtenberg H, Pesek J, et al. Continuous microfluidic synthesis of colloidal ultrasmall gold nanoparticles: *in situ* study of the early reaction stages and application for catalysis. React Chem Eng. 2017;2:876–884.
[65] Miyake T, Ueda T, Ikenaga N, et al. Synthesis of Fe2O3 in the capillary-tube reactor. J Mater Sci. 2005;40:5011–5013.
[66] Song Y, Modrow H, Henry LL, et al. Microfluidic synthesis of cobalt nanoparticles. Chem Mater. 2006;18:2817–2827.
[67] Frenz L, El Harrak A, Pauly M, et al. Droplet-based microreactors for the synthesis of magnetic iron oxide nanoparticles. Angew Chem Int Ed. 2008;47:6817–6820.
[68] Hassan AA, Sandre O, Cabuil V, et al. Synthesis of iron oxide nanoparticles in a microfluidic device: preliminary results in a coaxial flow millichannel. Chem Commun. 2008;74: 1783–1785.
[69] Song Y, Zhang T, Yang W, et al. Fine crystal structure transition of cobalt nanoparticles formed in a microfluidic reactor. Cryst Growth Des. 2008;8:3766–3772.
[70] Lee W-B, Weng C-H, Cheng F-Y, et al. Biomedical microdevices synthesis of iron oxide nanoparticles using a microfluidic system. Biomed Microdevices. 2009;11:161–171.
[71] Song Y, Henrys LL, Yang W. Stable amorphous cobalt nanoparticles formed by an in situ rapidly cooling microfluidic process. Langmuir. 2009;25:10209–10217.
[72] Kumar K, Nightingale AM, Krishnadasan SH, et al. Direct synthesis of dextran-coated superparamagnetic iron oxide nanoparticles in a capillary-based droplet reactor. J Mater Chem. 2012;22:4704–4708.
[73] Eluri R, Paul B. Synthesis of nickel nanoparticles by hydrazine reduction: mechanistic study and continuous flow synthesis. J Nanopart Res. 2012;14: 10115.

[74] Jiao M, Zeng J, Jing L, et al. Flow synthesis of biocompatible Fe3O4 nanoparticles: insight into the effects of residence time, fluid velocity, and tube reactor dimension on particle size distribution. Chem Mater. 2015;27:1299–1305.
[75] Xu L, Srinivasakannan C, Peng J, et al. Synthesis of nickel nanoparticles by aqueous reduction in continuous flow microreactor. Chem Eng Process. 2015;93:44–49.
[76] Lin S, Lin K, Lu D, et al. Preparation of uniform magnetic iron oxide nanoparticles by co-precipitation in a helical module microchannel reactor. J Environ Chem Eng. 2017;5:303–309.
[77] Uson L, Arruebo M, Sebastian V, et al. Single phase microreactor for the continuous, high-temperature synthesis of <4 Nm superparamagnetic iron oxide nanoparticles. Chem Eng J. 2018; doi:10.1016/j.cej.2017.12.024.
[78] Hayashi N, Sakai Y, Tsunoyama H, et al. Development of ultrafine multichannel microfluidic mixer for synthesis of bimetallic nanoclusters: catalytic application of highly monodisperse AuPd nanoclusters stabilized by poly(N -vinylpyrrolidone). Langmuir. 2014;30:10539–10547.
[79] Tofighi G, Gaur A, Doronkin DE, et al. Microfluidic synthesis of ultrasmall AuPd nanoparticles with a homogeneously mixed alloy structure in fast continuous flow for catalytic applications. J Phys Chem C. 2018; doi:10.1021/acs.jpcc.7b11383.
[80] Knauer A, Schneider S, Möller F, et al. Screening of plasmonic properties of composed metal nanoparticles by combinatorial synthesis in microfluid segment sequences. Chem Eng J. 2013;227:80–89.
[81] Yang C-G, Xu Z-R, Lee AP, et al. A microfluidic concentration-gradient droplet array generator for the production of multi-color nanoparticles. Lab Chip. 2013;13:2815–2820.
[82] Su YF, Kim H, Kovenklioglu S, et al. Continuous nanoparticle production by microfluidic-based emulsion, mixing and crystallization. J Solid State Chem. 2007;180:2625–2629.
[83] Ying Y, Chen G, Zhao Y, et al. A high throughput methodology for continuous preparation of monodispersed nanocrystals in microfluidic reactors. Chem Eng J. 2008;135:209–215.
[84] Li S, Xu J, Wang Y, et al. Controllable preparation of nanoparticles by drops and plugs flow in a microchannel device. Langmuir. 2008;24:4194–4199.
[85] Wang QA, Wang JX, Li M, et al. Large-scale preparation of barium sulphate nanoparticles in a high-throughput tube-in-tube microchannel reactor. Chem Eng J. 2009;149:473–478.
[86] Xu B-Y, Yang Z-Q, Xu J-J, et al. Liquid–gas dual phase microfluidic system for biocompatible CaCO3 hollow nanoparticles generation and simultaneous molecule doping. Chem Commun. 2012;48:11635–11637.
[87] Du L, Wang Y, Luo G. In situ preparation of hydrophobic CaCO3 nanoparticles in a gas-liquid microdispersion process. Particuology. 2013;11:421–427.
[88] Song Y, Henry LL. Nearly monodispersion CoSm alloy nanoparticles formed by an In-situ rapid cooling and passivating microfluidic process. Nanoscale Res Lett. 2009;4:1130–1134.
[89] Song Y, Doomes EE, Prindle J, et al. Investigations into sulfobetaine-stabilized Cu nanoparticle formation: toward development of a microfluidic synthesis. J Phys Chem B. 2005;109:9330–9338.
[90] Zhang Y, Jiang W, Wang L. Microfluidic synthesis of copper nanofluids. Microfluid Nanofluid. 2010;9:727–735.
[91] Song Y, Li R, Sun Q, et al. Controlled growth of Cu nanoparticles by a tubular microfluidic reactor. Chem Eng J. 2011;168:477–484.
[92] Ke T, Zeng X-F, Wang J-X, et al. Microfluidic synthesis of monodisperse Cu nanoparticles in aqueous solution. J Nanosci Nanotechnol. 2011;11:5154–5158.
[93] Xu L, Peng J, Srinivasakannan C, et al. Synthesis of copper nanoparticles by a T-shaped microfluidic device. RSC Adv. 2014;4:25155–25159.
[94] Wei X, Wang L. Microfluidic method for synthesizing Cu2O nanofluids. J Thermophys Heat Tr. 2010;24:445–448.
[95] Xu L, Srinivasakannan C, Peng J, et al. Microfluidic reactor synthesis and photocatalytic behavior of Cu@Cu2O nanocomposite. Appl Surf Sci. 2015;331:449–454.
[96] Xu L, Srinivasakannan C, Peng J, et al. Synthesis of Cu-CuO nanocomposite in microreactor and its application to photocatalytic degradation. J Alloy Compd. 2017;695:263–269.
[97] Shen X, Song Y, Li S, et al. Spatiotemporal-resolved nanoparticle synthesis via simple programmed microfluidic processes. RSC Adv. 2014;4:34179.
[98] Jung JH, Park TJ, Lee SY, et al. Homogeneous biogenic paramagnetic nanoparticle synthesis based on a microfluidic droplet generator. Angew Chem Int Ed. 2012;51:5634–5637.
[99] Abou-Hassan A, Bazzi R, Cabuil V. Multistep continuous-flow microsynthesis of magnetic and fluorescent γ-Fe2O3 @SiO2 core/shell nanoparticles. Angew Chem Int Ed. 2009;48:7180–7183.
[100] Abou-Hassan A, Dufrêchfer JF, Sandre O, et al. Fluorescence confocal laser scanning microscopy for Ph mapping in a coaxial flow microreactor: application in the synthesis of superparamagnetic nanoparticles. J Phys Chem C. 2009;113:18097–18105.
[101] Hoang PH, Park H, Kim DP. Ultrafast and continuous synthesis of unaccommodating inorganic nanomaterials in droplet- and ionic liquid-assisted microfluidic system. J Am Chem Soc. 2011;133:14765–14770.
[102] Song Y, Sun Q, Zhang T, et al. Synthesis of worm and chain-like nanoparticles by a microfluidic reactor process. J Nanopart Res. 2010;12:2689–2697.
[103] Torigoe K, Watanabe Y, Endo T, et al. Microflow reactor synthesis of palladium nanoparticles stabilized with poly(benzyl ether) dendron ligands. J Nanopart Res. 2010;12:951–960.
[104] Karim AM, Al Hasan N, Ivanov S, et al. Synthesis of 1 nm Pd nanoparticles in a microfluidic reactor: insights from in situ X-ray absorption fine structure spectroscopy and small-angle X-ray scattering. J Phys Chem C. 2015;119:13257–13267.
[105] Zhang D, Wu F, Peng M, et al. One-Step, facile and ultrafast synthesis of phase- and size-controlled Pt–Bi intermetallic nanocatalysts through continuous-flow microfluidics. J Am Chem Soc. 2015;137:6263–6269.
[106] Wang H, Nakamura H, Uehara M, et al. Preparation of titania particles utilizing the insoluble phase interface in a microchannel reactor. Chem Commun. 2002;38:1462–1463.

[107] Takagi M, Maki T, Miyahara M, et al. Production of titania nanoparticles by using a new microreactor assembled with same axle dual pipe. Chem Eng J. 2004;101:269–276.
[108] Cottam BF, Krishnadasan S, DeMello AJ, et al. Accelerated synthesis of titanium oxide nanostructures using microfluidic chips. Lab Chip. 2007;7:167–169.
[109] Eun TH, Kim SH, Jeong WJ, et al. Single-step fabrication of monodisperse TiO2 hollow spheres with embedded nanoparticles in microfluidic devices. Chem Mater. 2009;21:201–203.
[110] Baah D, Tigner J, Bean K, et al. Preparation of planar graded refractive index nanocomposites using microfluidics. Mater Sci Eng B. 2011;176:883–888.
[111] Koziej D, Floryan C, Sperling RA, et al. Microwave dielectric heating of non-aqueous droplets in a microfluidic device for nanoparticle synthesis. Nanoscale. 2013;5:5468–5475.
[112] Visaveliya N, Li S, Köhler JM. Heterogeneous nanoassembling: microfluidically prepared poly(methyl methacrylate) nanoparticles on Ag microrods and ZnO microflowers. Part Part Syst Char. 2013;30:614–623.
[113] Baruah A, Jindal A, Acharya C, et al. Microfluidic reactors for the morphology controlled synthesis and photocatalytic study of ZnO nanostructures. J Micromech Microeng. 2017;27:035013.
[114] Nightingale AM, de Mello JC. Microscale synthesis of quantum dots. J Mater Chem. 2010;20:8454–8463.
[115] Edel JB, Fortt R, DeMello JC, et al. Microfluidic routes to the controlled production of nanoparticles. Chem Commun. 2002;38:1136–1137.
[116] Shestopalov I, Tice JD, Ismagilov RF. Multi-step synthesis of nanoparticles performed on millisecond time scale in a microfluidic droplet-based system. Lab Chip. 2004;4:316–321.
[117] Hung L-H, Choi KM, Tseng W-Y, et al. Alternating droplet generation and controlled dynamic droplet fusion in microfluidic device for CdS nanoparticle synthesis. Lab Chip. 2006;6:174–178.
[118] Dai J, Yang X, Hamon M, et al. Particle size controlled synthesis of CdS nanoparticles on a microfluidic chip. Chem Eng J. 2015;280:385–390.
[119] Nakamura H, Yamaguchi Y, Miyazaki M, et al. Preparation of CdSe nanocrystals in a micro-flow-reactor. Chem Commun. 2002;38:2844–2845.
[120] Nakamura H, Tashiro A, Yamaguchi Y, et al. Application of a microfluidic reaction system for CdSe nanocrystal preparation: their growth kinetics and photoluminescence analysis. Lab Chip. 2004;4:237–240.
[121] Luan W, Yang H, Tu S, et al. Open-to-air synthesis of monodisperse CdSe nanocrystals via microfluidic reaction and its kinetics. Nanotechnology. 2007;18:175603.
[122] Nightingale AM, Bannock JH, Krishnadasan SH, et al. Large-scale synthesis of nanocrystals in a multichannel droplet reactor. J Mater Chem A. 2013;1:4067–4076.
[123] Krishnadasan S, Tovilla J, Vilar R, et al. On-line analysis of CdSe nanoparticle formation in a continuous flow chip-based microreactor. J Mater Chem. 2004;14:2655–2660.
[124] Wang H, Tashiro A, Nakamura H, et al. Synthesis of CdSe magic-sized nanocluster and its effect on nanocrystal preparation in a microfluidic reactor. J Mater Res. 2004;19:3157–3161.
[125] Wang H, Nakamura H, Uehara M, et al. Highly luminescent CdSe/ZnS nanocrystals synthesized using a single-molecular ZnS source in a microfluidic reactor. Adv Funct Mater. 2005;15:603–608.
[126] Yang H, Luan W, Tu S, et al. Synthesis of nanocrystals via microreaction with temperature gradient: towards separation of nucleation and growth. Lab Chip. 2008;8:451–455.
[127] Wan Z, Yang H, Luan W, et al. Facile synthesis of monodisperse CdS nanocrystals via microreaction. Nanoscale Res Lett. 2010;5:130–137.
[128] Luan W, Yang H, Fan N, et al. Synthesis of efficiently green luminescent CdSe/ZnS nanocrystals via microfluidic reaction. Nanoscale Res Lett. 2008;3:134–139.
[129] Marre S, Park J, Rempel J, et al. Supercritical continuous-microflow synthesis of narrow size distribution quantum dots. Adv Mater. 2008;20:4830–4834.
[130] Kikkeri R, Laurino P, Odedra A, et al. Synthesis of carbohydrate-functionalized quantum dots in microreactors. Angew Chem Int Ed. 2010;49:2054–2057.
[131] Sounart TL, Safier PA, Voigt JA, et al. Spatially-resolved analysis of nanoparticle nucleation and growth in a microfluidic reactor. Lab Chip. 2007;7:908–915.
[132] Hu S, Zeng S, Zhang B, et al. Preparation of biofunctionalized quantum dots using microfluidic chips for bioimaging. Analyst. 2014;139:4681–4690.
[133] Toyota A, Nakamura H, Ozono H, et al. Combinatorial synthesis of CdSe nanoparticles using microreactors. J Phys Chem C. 2010;114:7527–7534.
[134] Lignos I, Stavrakis S, Kilaj A, et al. Millisecond-timescale monitoring of PbS nanoparticle nucleation and growth using droplet-based microfluidics. Small. 2015;11:4009–4017.
[135] Yen BKH, Stott NE, Jensen KF, et al. A continuous-flow microcapillary reactor for the preparation of a size series of CdSe nanocrystals. Adv Mater. 2003;15:1858–1862.
[136] Chan EM, Mathies RA, Alivisatos AP. Size-controlled growth of CdSe nanocrystals in microfluidic reactors. Nano Lett. 2003;3:199–201.
[137] Wang H, Li X, Uehara M, et al. Continuous synthesis of CdSe-ZnS composite nanoparticles in a microfluidic reactor. Chem Commun. 2004;56:48–49.
[138] Yen BKH, Günther A, Schmidt MA, et al. A microfabricated gas-liquid segmented flow reactor for high-temperature synthesis: the case of CdSe quantum dots. Angew Chem Int Ed. 2005;44:5447–5451.
[139] Krishnadasan S, Brown RJC, DeMello AJ, et al. Intelligent routes to the controlled synthesis of nanoparticles. Lab Chip. 2007;7:1434–1441.
[140] Yang H, Fan N, Luan W, et al. Synthesis of monodisperse nanocrystals via microreaction: open-to-air synthesis with oleylamine as a coligand. Nanoscale Res Lett. 2009;4:344–352.
[141] Uehara M, Nakamura H, Maeda H. Preparation of ZnS/CdSe/ZnS quantum dot quantum well by using a microfluidic reactor. J Nanosci Nanotechnol. 2009;9:577–583.
[142] Yang H, Luan W, Tu ST, et al. High-temperature synthesis of CdSe nanocrystals in a serpentine microchannel: wide size tunability achieved under a short residence time. Cryst Growth Des. 2009;9:1569–1574.

[143] Nightingale AM, de Mello JC. Controlled synthesis of III-V quantum dots in microfluidic reactors. ChemPhysChem. 2009;10:2612–2614.
[144] Kwon BH, Lee KG, Park TJ, et al. Continuous in situ synthesis of ZnSe/ZnS core/shell quantum dots in a microfluidic reaction system and its application for light-emitting diodes. Small. 2012;8:3257–3262.
[145] Lignos I, Protesescu L, Stavrakis S, et al. Facile droplet-based micro fluidic synthesis of monodisperse IV − VI semiconductor nanocrystals with coupled in-line NIR fluorescence detection. Chem Mater. 2014;26:2975–2982.
[146] Tian Z-H, Wang Y-J, Xu J-H, et al. Intensification of nucleation stage for synthesizing high quality CdSe quantum dots by using preheated precursors in microfluidic devices. Chem Eng J. 2016;302:498–502.
[147] Tian Z-H, Xu J-H, Wang Y-J, et al. Microfluidic synthesis of monodispersed CdSe quantum dots nanocrystals by using mixed fatty amines as ligands. Chem Eng J. 2016;285:20–26.
[148] Hong L, Cheung TL, Rao N, et al. Millifluidic synthesis of cadmium sulfide nanoparticles and their application in bioimaging. RSC Adv. 2017;7:36819–36832.
[149] Wang J, Zhao H, Zhu Y, et al. Shape-controlled synthesis of CdSe nanocrystals via a programmed microfluidic process. J Phys Chem C. 2017;121:3567–3572.
[150] Swain B, Hong MH, Kang L, et al. Optimization of CdSe nanocrystals synthesis with a microfluidic reactor and development of combinatorial synthesis process for industrial production. Chem Eng J. 2017;308:311–321.
[151] Kwak CH, Park JP, Lee SS, et al. Droplet-based microfluidic reactor for synthesis of size-controlled CdSe quantum dots. J Nanosci Nanotechnol. 2018;18:1339–1342.
[152] Hao N, Li L, Tang F. Shape matters when engineering mesoporous silica-based nanomedicines. Biomater Sci. 2016;4:575–591.
[153] Hao N, Chen X, Jayawardana KW, et al. Shape control of mesoporous silica nanomaterials templated with dual cationic surfactants and their antibacterial activities. Biomater Sci. 2016;4:87–91.
[154] Hao NJ, Yang HH, Li LF, et al. The shape effect of mesoporous silica nanoparticles on intracellular reactive oxygen species in A375 cells. New J Chem. 2014;38:4258–4266.
[155] Hao N, Chen X, Jeon S, et al. Carbohydrate-conjugated hollow oblate mesoporous silica nanoparticles as nanoantibiotics to target mycobacteria. Adv Healthc Mater. 2015;4:2797–2801.
[156] Hao N, Tang F, Li L. MCM-41 mesoporous silica sheet with ordered perpendicular nanochannels for protein delivery and the assembly of Ag nanoparticles in catalytic applications. Microporous Mesoporous Mater. 2015;218:223–227.
[157] Hao N, Jayawardana KW, Chen X, et al. One-step synthesis of amine-functionalized hollow mesoporous silica nanoparticles as efficient antibacterial and anticancer materials. ACS Appl Mater Interfaces. 2015;7:1040–1045.
[158] Khan SA, Günther A, Schmidt MA, et al. Microfluidic synthesis of colloidal silica. Langmuir. 2004;20:8604–8611.
[159] Günther A, Khan SA, Thalmann M, et al. Transport and reaction in microscale segmented gas-liquid flow. Lab Chip. 2004;4:278–286.
[160] He P, Greenway G, Haswell SJ. Microfluidic synthesis of silica nanoparticles using polyethylenimine polymers. Chem Eng J. 2011;167:694–699.
[161] Gutierrez L, Gomez L, Irusta S, et al. Comparative study of the synthesis of silica nanoparticles in micromixer-microreactor and batch reactor systems. Chem Eng J. 2011;171:674–683.
[162] Chung CK, Shih TR, Chang CK, et al. Design and experiments of a short-mixing-length baffled microreactor and its application to microfluidic synthesis of nanoparticles. Chem Eng J. 2011;168:790–798.
[163] Carroll NJ, Rathod SB, Derbins E, et al. Droplet-based microfluidics for emulsion and solvent evaporation synthesis of monodisperse mesoporous silica microspheres. Langmuir. 2008;24:658–661.
[164] Lee I, Yoo Y, Cheng Z, et al. Generation of monodisperse mesoporous silica microspheres with controllable size and surface morphology in a microfluidic device. Adv Funct Mater. 2008;18:4014–4021.
[165] Jeong W, Choi M, Lim CH, et al. Microfluidic synthesis of atto-liter scale double emulsions toward ultrafine hollow silica spheres with hierarchical pore networks. Lab Chip. 2012;12:5262–5271.
[166] Carroll NJ, Crowder PF, Pylypenko S, et al. Microfluidic synthesis of monodisperse nanoporous oxide particles and control of hierarchical pore structure. ACS Appl Mater Interfaces. 2013;5:3524–3529.
[167] Ng TN, Chen XQ, Yeung KL. Direct manipulation of particle size and morphology of ordered mesoporous silica by flow synthesis. RSC Adv. 2015;5:13331–13340.
[168] Li D, Guan Z, Zhang W, et al. Synthesis of uniform-size hollow silica microspheres through interfacial polymerization in monodisperse water-in-oil droplets. ACS Appl Mater Interfaces. 2010;2:2711–2714.
[169] Tachibana M, Engl W, Panizza P, et al. Combining sol-gel chemistry and millifluidic toward engineering microporous silica ceramic final sizes and shapes: an integrative chemistry approach. Chem Eng Process. 2008;47:1317–1322.
[170] Fang A, Gaillard C, Douliez JP. Template-free formation of monodisperse doughnut-shaped silica microparticles by droplet-based microfluidics. Chem Mater. 2011;23:4660–4662.
[171] Zhao CX, Middelberg APJ. Microfluidic synthesis of monodisperse hierarchical silica particles with raspberry-like morphology. RSC Adv. 2013;3:21227–21230.
[172] Lee D, Weitz DA. Nonspherical colloidosomes with multiple compartments from double emulsions. Small. 2009;5:1932–1935.
[173] Chokkalingam V, Weidenhof B, Krämer M, et al. Optimized droplet-based microfluidics scheme for sol-gel reactions. Lab Chip. 2010;10:1700–1705.
[174] Lee MH, Prasad V, Lee D. Microfluidic fabrication of stable nanoparticle-shelled bubbles. Langmuir. 2010;26:2227–2230.
[175] Chokkalingam V, Weidenhof B, Krämer M, et al. Template-free preparation of mesoporous silica spheres through optimized microfluidics. ChemPhysChem. 2010;11:2091–2095.
[176] Wacker JB, Lignos I, Parashar VK, et al. Controlled synthesis of fluorescent silica nanoparticles inside microfluidic droplets. Lab Chip. 2012;12:3111–3116.
[177] Ju M, Ji X, Wang C, et al. Preparation of solid, hollow, hole-shell and asymmetric silica microspheres by microfluidic-assisted solvent extraction process. Chem Eng J. 2014;250:112–118.

[178] Bchellaoui N, Hayat Z, Mami M, et al. Microfluidic-assisted formation of highly monodisperse and mesoporous silica soft microcapsules. Sci Rep. 2017;7:1278.
[179] Hao N, Nie Y, Tadimety A, et al. Microfluidics-mediated self-template synthesis of anisotropic hollow ellipsoidal mesoporous silica nanomaterials. Mater Res Lett. 2017;5:584–590.
[180] Nie Y, Hao N, Zhang XJ. Ultrafast synthesis of multifunctional submicrometer hollow silica spheres in microfluidic spiral channels. Sci Rep. 2017;7:3987.
[181] Hao N, Nie Y, Zhang XJ. Microfluidic flow synthesis of functional mesoporous silica nanofibers with tunable aspect ratios. ACS Sustainable Chem Eng. 2018;6:1522–1526. doi:10.1021/acssuschemeng.7b03527
[182] Park JI, Saffari A, Kumar S, et al. Microfluidic synthesis of polymer and inorganic particulate materials. Annu Rev Mater Res. 2010;40:415–443.
[183] Tao S, Yang M, Chen H, et al. Microfluidic synthesis of Ag@Cu2O core-shell nanoparticles with enhanced photocatalytic activity. J Colloid Interf Sci. 2017;486:16–26.
[184] Tao S, Yang M, Chen H, et al. Continuous synthesis of hedgehog-like Ag–ZnO nanoparticles in a two-stage microfluidic system. RSC Adv. 2016;6:45503–45511.
[185] Sander JS, Studart AR. Monodisperse functional colloidosomes with tailored nanoparticle shells. Langmuir. 2011;27:3301–3307.
[186] Köhler JM, Romanus H, Hübner U, et al. Formation of star-like and core-shell AuAg nanoparticles during two- and three-step preparation in batch and in microfluidic systems. J Nanomater. 2007;2007:1–7.
[187] Knauer A, Thete A, Li S, et al. Au/Ag/Au double shell nanoparticles with narrow size distribution obtained by continuous micro segmented flow synthesis. Chem Eng J. 2011;166:1164–1169.
[188] Fang J, Evans CW, Willis GJ, et al. Sequential microfluidic flow synthesis of CePO4 nanorods decorated with emission tunable quantum dots. Lab Chip. 2010;10:2579–2582.
[189] Straß A, Maier R, Güttel R. Continuous synthesis of nanostructured Co3O4@SiO2 core-shell particles in a laminar-flow reactor. Chem Ing Tech. 2017;89:963–967.
[190] Weng CH, Huang CC, Yeh CS, et al. Synthesis of hollow, magnetic Fe/Ga-based oxide nanospheres using a bubble templating method in a microfluidic system. Microfluid Nanofluid. 2009;7:841–848.
[191] Lee S-K, Liu X, Sebastián Cabeza V, et al. Synthesis, assembly and reaction of a nanocatalyst in microfluidic systems: a general platform. Lab Chip. 2012;12:4080–4084.
[192] Song Y, Ji S, Song Y, et al. In situ redox microfluidic synthesis of core–shell nanoparticles and their long-term stability. J Phys Chem C. 2013;117:17274–17284.
[193] Han DJ, Jung JH, Choi JS, et al. Synthesis of a 3D graphite microball using a microfluidic droplet generator and its polymer composite with core–shell structure. Lab Chip. 2013;13:4006–4010.
[194] Zhu X, Zhang Q, Li Y, et al. Facile crystallization control of LaF3/LaPO4:Ce, Tb nanocrystals in a microfluidic reactor using microwave irradiation. J Mater Chem. 2010;20:1766–1771.
[195] Kataoka S, Takeuchi Y, Harada A, et al. Microreactor containing platinum nanoparticles for nitrobenzene hydrogenation. Appl Catal A. 2012;427–428:119–124.
[196] Duraiswamy S, Khan SA. Plasmonic nanoshell synthesis in microfluidic composite foams. Nano Lett. 2010;10:3757–3763.
[197] Rahman MT, Krishnamurthy PG, Parthiban P, et al. Dynamically tunable nanoparticle engineering enabled by short contact-time microfluidic synthesis with a reactive gas. RSC Adv. 2013;3:2897–2900.
[198] Hassan N, Cabuil V, Abou-Hassan A. Continuous multistep microfluidic assisted assembly of fluorescent, plasmonic, and magnetic nanostructures. Angew Chem Int Ed. 2013;52:1994–1997.
[199] Khan SA, Jensen KF. Microfluidic synthesis of titania shells on colloidal silica. Adv Mater. 2007;19:2556–2560.
[200] Lan W, Li S, Xu J, et al. Synthesis of titania-silica core-shell microspheres via a controlled interface reaction in a microfluidic device. Langmuir. 2011;27:13242–13247.
[201] Shang L, Shangguan F, Cheng Y, et al. Microfluidic generation of magnetoresponsive Janus photonic crystal particles. Nanoscale. 2013;5:9553–9557.
[202] Singh A, Limaye M, Singh S, et al. A facile and fast approach for the synthesis of doped nanoparticles using a microfluidic device. Nanotechnology. 2008;19:245613.
[203] Yang CH, Wang LS, Chen SY, et al. Microfluidic assisted synthesis of silver nanoparticle–chitosan composite microparticles for antibacterial applications. Int J Pharm. 2016;510:493–500.
[204] Kim Y, Fay F, Cormode DP, et al. Single step reconstitution of multifunctional high-density lipoprotein-derived nanomaterials using microfluidics. ACS Nano. 2013;7:9975–9983.
[205] Chang Z, Serra CA, Bouquey M, et al. Multiscale materials from microcontinuous-flow synthesis: ZnO and Au nanoparticle-filled uniform and homogeneous polymer microbeads. Nanotechnology. 2010;21:015605.
[206] He J, Wang L, Wei Z, et al. Vesicular self-assembly of colloidal amphiphiles in microfluidics. ACS Appl Mater Interfaces. 2013;5:9746–9751.
[207] Groß GA, Hamann C, Günther M, et al. Formation of polymer and nanoparticle doped polymer minirods by use of the microsegmented flow principle. Chem Eng Technol. 2007;30:341–346.
[208] Wang Q, Zhang D, Yang X, et al. Atom-economical in situ synthesis of BaSO4 as imaging contrast agents within poly(N-isopropylacrylamide) microgels using one-step droplet microfluidics. Green Chem. 2013;15:2222–2229.
[209] Schabas G, Wang CW, Oskooei A, et al. Formation and shear-induced processing of quantum dot colloidal assemblies in a multiphase microfluidic chip. Langmuir. 2008;24:10596–10603.
[210] Wang C-W, Oskooei A, Sinton D, et al. Controlled self-assembly of quantum dot–block copolymer colloids in multiphase microfluidic reactors. Langmuir. 2010;26:716–723.
[211] Tran TH, Nguyen CT, Kim D, et al. Microfluidic approach for highly efficient synthesis of heparin-based bioconjugates for drug delivery. Lab Chip. 2012;12:589–594.
[212] Chang J-Y, Yang C-H, Huang K-S. Microfluidic assisted preparation of CdSe/ZnS nanocrystals encapsulated into poly(DL-lactide- co -glycolide) microcapsules. Nanotechnology. 2007;18:305305.

[213] Valencia PM, Basto PA, Zhang L, et al. Single-step assembly of homogenous lipid-polymeric and lipid-quantum dot nanoparticles enabled by microfluidic rapid mixing. ACS Nano. 2010;4:1671–1679.
[214] Zhao Y, Shum HC, Chen H, et al. Microfluidic generation of multifunctional quantum dot barcode particles. J Am Chem Soc. 2011;133:8790–8793.
[215] Chen Y, Dong PF, Xu JH, et al. Microfluidic generation of multicolor quantum-dot-encoded core-shell microparticles with precise coding and enhanced stability. Langmuir. 2014;30:8538–8542.
[216] Seth A, Béalle G, Santanach-Carreras E, et al. Design of vesicles using capillary microfluidic devices: from magnetic to multifunctional vesicles. Adv Mater. 2012;24:3544–3548.
[217] Wang W, Yang C, Cui XQ, et al. Droplet microfluidic preparation of au nanoparticles-coated chitosan microbeads for flow-through surface-enhanced Raman scattering detection. Microfluid Nanofluid. 2010;9:1175–1183.
[218] Lan W, Li S, Xu J, et al. Controllable preparation of nanoparticle-coated chitosan microspheres in a co-axial microfluidic device. Lab Chip. 2011;11:652–657.
[219] Hwang DK, Dendukuri D, Doyle PS. Microfluidic-based synthesis of non-spherical magnetic hydrogel microparticles. Lab Chip. 2008;8:1640–1647.
[220] Hasani-Sadrabadi MM, Dashtimoghadam E, Bahlakeh G, et al. On-chip synthesis of fine-tuned bone-seeking hybrid nanoparticles. Nanomedicine. 2015;10:3431–3449.
[221] Lin YS, Huang KS, Yang CH, et al. Microfluidic synthesis of microfibers for magnetic-responsive controlled drug release and cell culture. PLoS One. 2012;7:4–11.
[222] Paseta L, Seoane B, Julve D, et al. Accelerating the controlled synthesis of metal–organic frameworks by a microfluidic approach: a nanoliter continuous reactor. ACS Appl Mater Interfaces. 2013;5:9405–9410.
[223] Faustini M, Kim J, Jeong G, et al. Microfluidic approach toward continuous and ultrafast synthesis of metal − organic framework crystals and hetero structures in confined microdroplets. J Am Chem Soc. 2013;135:14619–14626.
[224] Nam JO, Kim J, Jin SH, et al. Microfluidic preparation of a highly active and stable catalyst by high performance of encapsulation of polyvinylpyrrolidone (PVP)-Pt nanoparticles in microcapsules. J Colloid Interf Sci. 2016;464:246–253.
[225] Prasad N, Perumal J, Choi CH, et al. Generation of monodisperse inorganic-organic janus microspheres in a microfluidic device. Adv Funct Mater. 2009;19:1656–1662.
[226] Lan W, Li S, Xu J, et al. One-step synthesis of chitosan-silica hybrid microspheres in a microfluidic device. Biomed Microdevices. 2010;12:1087–1095.
[227] Hwang H, Kim S-H, Yang S-M. Microfluidic fabrication of SERS-active microspheres for molecular detection. Lab Chip. 2011;11:87–92.
[228] Park J, Nie Z, Kumachev A, et al. A microfluidic approach to chemically driven assembly of colloidal particles at Gas-liquid interfaces. Angew Chem Int Ed. 2009;121:5404–5408.
[229] Seo M, Gorelikov I, Williams R, et al. Microfluidic assembly of monodisperse, nanoparticle-incorporated perfluorocarbon microbubbles for medical imaging and therapy. Langmuir. 2010;26:13855–13860.
[230] Liu D, Herranz-Blanco B, Mäkilä E, et al. Microfluidic templated mesoporous silicon–solid lipid microcomposites for sustained drug delivery. ACS Appl Mater Interfaces. 2013;5:12127–12134.
[231] Lan W, Li S, Xu J, et al. A one-step microfluidic approach for controllable preparation of nanoparticle-coated patchy microparticles. Microfluid Nanofluid. 2012;13:491–498.
[232] Liu D, Zhang H, Mäkilä E, et al. Microfluidic assisted one-step fabrication of porous silicon@acetalated dextran nanocomposites for precisely controlled combination chemotherapy. Biomaterials. 2015;39:249–259.
[233] Gerver RE, Gómez-Sjöberg R, Baxter BC, et al. Programmable microfluidic synthesis of spectrally encoded microspheres. Lab Chip. 2012;12:4716–4723.
[234] Shepherd RF, Conrad JC, Rhodes SK, et al. Microfluidic assembly of homogeneous and Janus colloid-filled hydrogel granules. Langmuir. 2006;22:8618–8622.
[235] Chen Y, Nurumbetov G, Chen R, et al. Multicompartmental Janus microbeads from branched polymers by single-emulsion droplet microfluidics. Langmuir. 2013;29:12657–12662.
[236] Khan IU, Serra CA, Anton N, et al. Production of nanoparticle drug delivery systems with microfluidics tools. Expert Opin Drug Deliv. 2014;12:1–16.
[237] Riahi R, Tamayol A, Shaegh SAM, et al. Microfluidics for advanced drug delivery systems. Curr Opin Chem Eng. 2015;7:101–112.
[238] Björnmalm M, Yan Y, Caruso F. Engineering and evaluating drug delivery particles in microfluidic devices. J Control Release. 2014;190:139–149.
[239] Zhao C-X. Multiphase flow microfluidics for the production of single or multiple emulsions for drug delivery. Adv Drug Deliv Rev. 2013;65:1420–1446.
[240] Yang S, Guo F, Kiraly B, et al. Microfluidic synthesis of multifunctional Janus particles for biomedical applications. Lab Chip. 2012;12:2097–2102.
[241] Hao NJ, Liu HY, Li LL, et al. In vitro degradation behavior of silica nanoparticles under physiological conditions. J Nanosci Nanotechnol. 2012;12:6346–6354.
[242] Hao NJ, Nie Y, Zhang XJ. Biomimetic hierarchical walnut kernel-like and erythrocyte-like mesoporous silica nanomaterials: controllable synthesis and versatile applications. Microporous Mesoporous Mater. 2018;261:144–149.
[243] Hao N, Li L, Zhang Q, et al. The shape effect of PEGylated mesoporous silica nanoparticles on cellular uptake pathway in Hela cells. Microporous Mesoporous Mater. 2012;162:14–23.
[244] Hao N, Li L, Tang F. Facile preparation of ellipsoid-like MCM-41 with parallel channels along the short axis for drug delivery and assembly of Ag nanoparticles for catalysis. J Mater Chem A. 2014;2:11565–11568.
[245] Hao NJ, Chorsi HT, Zhang XJ. Hierarchical lotus leaf-like mesoporous silica material with unique bilayer and hollow sandwich-like folds: synthesis, mechanism, and applications. ACS Sustain Chem Eng. 2017;5:2044–2049.
[246] Valencia PM, Farokhzad OC, Karnik R, et al. Microfluidic technologies for accelerating the clinical translation of nanoparticles. Nat Nanotechnol. 2012;7:623–629.